Corresponding author:
Ülo Suursaar
ulo.suursaar@ut.ee

Morphostratigraphy and chronology of depositional and erosional events at the Järve scarp (Saaremaa, western Estonia) over the past 2000 years

Ülo Suursaar[a,b], Katre Luik[a], Alar Rosentau[c], Helena Alexanderson[d], Reimo Rivis[a], Tiit Vaasma[a], Egert Vandel[a], Kadri Vilumaa[a], Donatas Pupienis[e] and Hannes Tõnisson[a]

[a] Institute of Ecology, School of Natural Sciences and Health, Tallinn University, Narva mnt 29, 10120 Tallinn, Estonia

[b] Estonian Marine Institute, Faculty of Science and Technology, University of Tartu, Mäealuse 14, 12618 Tallinn, Estonia

[c] Institute of Ecology and Earth Sciences, Faculty of Science and Technology, University of Tartu, J. Liivi 2, 50409 Tartu, Estonia

[d] Department of Geology, Lund University, Sölvegatan 12, 22362 Lund, Sweden

[e] Institute of Geosciences, Faculty of Chemistry and Geosciences, Vilnius University, M. K. Čiurlionio g. 21, 03101 Vilnius, Lithuania

ABSTRACT

Influenced by climate warming and sea-level rise, seacoasts in many parts of the world are undergoing regime shifts, including increased coastal erosion in the southeastern Baltic Sea. The aim of this study is to reconstruct the depositional and erosional history of the Järve coastal scarp using sediment stratigraphy, new luminescence and radiocarbon dates, ground-penetrating radar, and LiDAR data. The seaward ridge, where the 3.5-m-high sandy scarp is located, began to form around 1600 years ago, in front of a 3500–4000-year-old palaeospit system that developed through sediment accumulation and postglacial uplift. The lower section of the outcrop was deposited in the shallow nearshore zone, where underwater sandbars acted as nuclei for spit formation. Darker sediment layers and variations in lamination patterns reflect changes in sediment sources and storm activity. Above the marine-deposited sandy layers lies a thin aeolian unit, which is only weakly developed at the Järve outcrop. Dune features occur only in a few blowouts, likely associated with the Little Ice Age (~1300–1850 CE) and anthropogenic vegetation disturbance, such as logging or slash-and-burn agriculture. Over the past ~100 years, the formerly emergent system of beach ridges and spits has shifted to an erosional regime. The earlier relative sea-level fall has ceased, seasonal sea ice is diminishing, the impacts of winter storms are intensifying, and the scarp is retreating. This study demonstrates how global changes are manifested on seacoasts at a local scale and highlights methodological difficulties in using seashells for coastal stratigraphic dating.

1. Introduction

Coastal accumulation landforms, such as spits, beach ridges, and foredune plains, serve as morphological and sedimentary archives of past climatological and oceanographic conditions (Buynevich et al. 2004, 2023; Tamura 2012; Dougherty 2014; Clemmensen et al. 2015; Kalińska et al. 2024). Using various stratigraphic and chronological methods, GIS-based analysis of LiDAR elevation data, and ground-penetrating radar (GPR) surveys, it is possible to reconstruct the successive stages of the development of these landforms in response to forcing conditions and sediment availability (Rosentau et al. 2013; Muru et al. 2018; Suursaar et al. 2022; Luik et al. 2025). Deciphering signs of environmental change in coastal landscapes is especially important in the current era of rising sea levels, changing climate, and their extensive impacts on society (e.g. IPCC 2021; Costas 2022; Różyński 2023).

In many parts of the world, the coastal stretches that until recently experienced a net seaward progradation, either due to sediment accretion or uplift-driven land emergence, may now be entering a phase of coastal erosion (e.g. Morton et al. 2004;

Weisse et al. 2021). Such shifts can occur due to relative sea-level rise or a sediment deficit of variable origin. For instance, on the coasts of the southern and southeastern Baltic Sea, adverse effects of coastal erosion and dune destruction have been reported since at least the 1990s (Eberhards and Saltupe 1995; Furmanczyk and Musielak 2002; Różyński 2023; Uścinowicz et al. 2024). On the seacoasts of Estonia, the present-day isostatic postglacial uplift component (1.3–3.5 mm/a; Suursaar and Kall 2018; Vestøl et al. 2019) has so far mostly exceeded the eustatic global sea-level (GSL) rise component (~1.7 mm/a during the 20th century; IPCC 2021). However, according to recent satellite-based estimates, the GSL has accelerated to ~3.4 mm/a between 1993 and 2024 (Willis et al. 2024). Consequently, Estonia's land surface area is no longer increasing as it did throughout the Middle and Late Holocene (over the past ~7000 years). In combination with changing storminess and decreasing ice cover (Jaagus and Suursaar 2013; Suursaar et al. 2015; Tõnisson et al. 2024a), the seacoasts are becoming increasingly erosional. Such coastal systems offer a unique opportunity to study past climate events (e.g. storms) and regime shifts by juxtaposing relict accretional landforms with recent erosional evidence (e.g. Buynevich et al. 2023).

The Järve coast in southern Saaremaa (Fig. 1) is an illustrious example of such shifts, where a system of palaeo-spits emerged from the sea ~3500 years ago. Over time, the barrier gradually grew and fused with the main part of Saaremaa due to postglacial uplift and sediment accretion, eventually becoming erosional on its southern side. This transition likely occurred by the 1940s–1950s, as the local relative sea level began to rise at Järve and the duration of seasonal ice cover significantly decreased (Luik et al. 2024a; Tõnisson et al. 2024a; Suursaar et al. 2025). A photo (fig. 10B in Luik et al. 2025) shows the 4-m-high Järve scarp streaked with several near-horizontal dark layers, which could hypothetically reflect shifts in the formation of the palaeospit, and possibly past storm events. However, the age, origin, and lithological characteristics of these streaks were not analysed in detail in that otherwise extensive study. Based on previous dating from the Järve interior (Luik et al. 2025), it was suggested that the age of landforms that run along the present day coastline is ~2000 years at Järve (Fig. 1). However, there was at least a 1500-year-long gap in dating due to a more recent transition from accretion to coastal erosion.

To fill the gap revealed by previous studies (Orviku 2006; Luik et al. 2025), additional fieldwork was conducted in

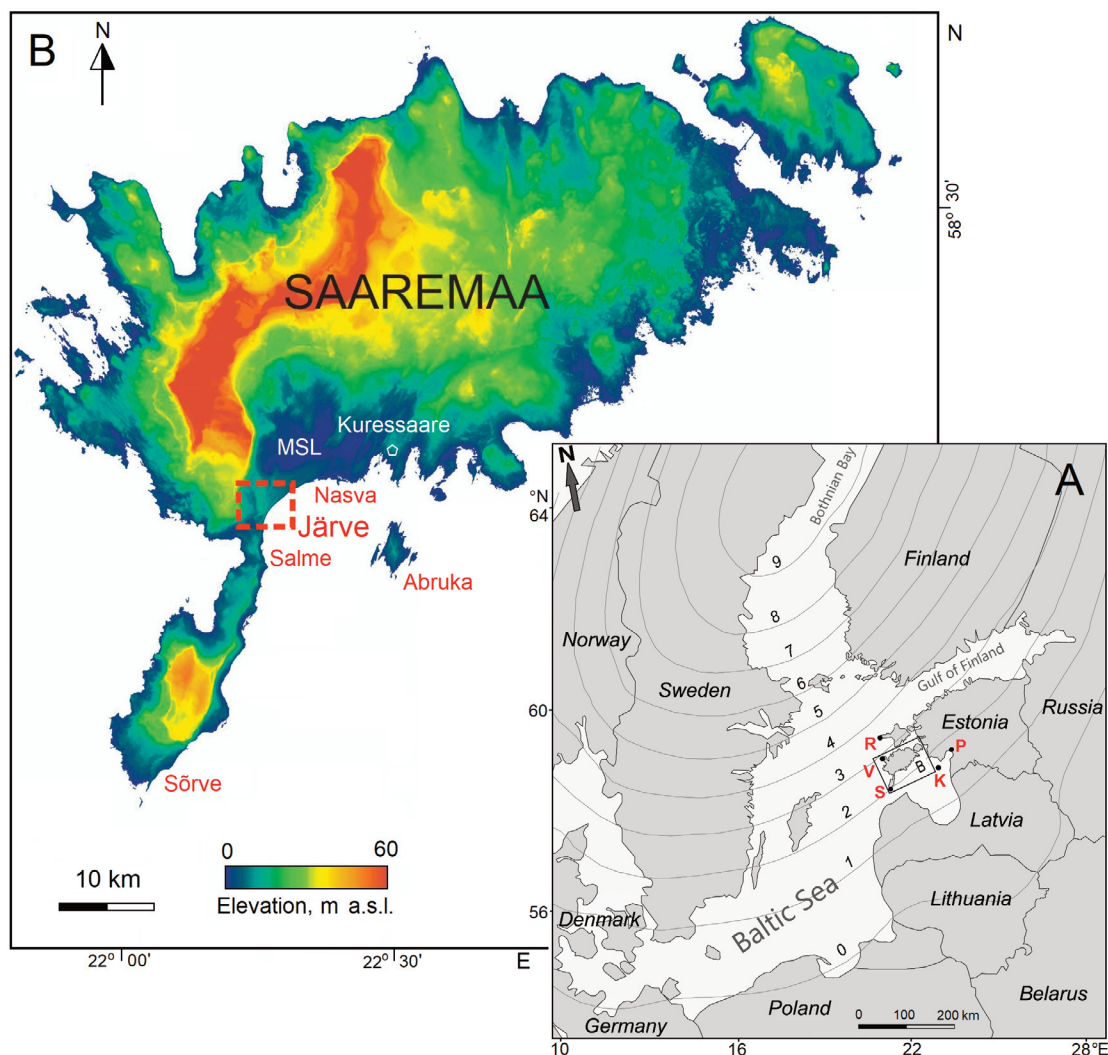**Fig. 1.** Location of Saaremaa Island in the Baltic Sea with the present-day isobases (mm/a) according to the NKG2016LU_lev land uplift model (Vestøl et al. 2019). Coastal hydrometeorological stations (A): R – Ristna, V – Vilsandi, S – Sõrve, K – Kihnu, P – Pärnu. LiDAR-based elevation map of Saaremaa (B) with the Järve area (see Fig. 2) marked with a rectangle. MSL – Mullutu-Suurlaht Lagoon.

December 2024 to further investigate the geomorphic history revealed by the Järve outcrop. The aims of this study are: (1) to reconstruct the depositional and erosional events of the Järve palaeospit based on new optically stimulated luminescence (OSL) and radiocarbon (^{14}C) dates, as well as a lithological description of the outcrop; (2) to interpret the occurrences of different layers (streaks) in the outcrop in relation to possible climatic and oceanographic shifts or extreme events; and (3) to discuss the processes related to the transition from coastal progradation/accretion to erosion, which is expected to occur at an accelerating pace in many areas around the world.

2. Materials and methods

2.1. Geological and climatological setting of the study area

The study area, located along the Järve coast in Saaremaa, Estonia, is a dynamic coastal system that has been shaped by postglacial land emergence, coastal progradation, and sedimentary processes over the past 4000 years (i.e. roughly the Limnea Sea stage of the Baltic Sea; e.g. Hang et al. 2020). Saaremaa, the fourth largest island in the Baltic Sea, is part of the West Estonian Archipelago and currently covers an area of ~2673 km². Geologically, Saaremaa lies at the edge of the Fennoscandian Shield, where the crystalline basement consists mainly of metamorphic rocks and granite (Kalm 2006). This basement is covered by Silurian limestone and a

relatively thin Quaternary sediment layer. The area's subsequent geological evolution was closely related to the development stages of the Baltic Sea basin following the Late Weichselian glaciation and subsequent shoreline changes driven by eustatic sea-level fluctuations, postglacial rebound, and alteration between oceanic and dammed-up limnic conditions (Kalm 2006; Rosentau et al. 2009, 2020; Andrén et al. 2011). In the study area, falls in water level were interrupted by the Lake Ancylus and Littorina Sea transgressions (~10 700–10 200 and ~8500–7300 years ago, respectively; Saarse et al. 2009; Hang et al. 2020; Harff et al. 2020). Filling a buried ancient valley, the Quaternary cover below the Järve area is relatively thick (20–40 m). Serving as a local depot for sandy sediment, it is overlain by more recent moraine and laminated Littorina sediment (Suuroja et al. 2020). Subsequently, this sedimentary complex has been raised by glacio-isostatic uplift to the zone of active coastal processes and ultimately above sea level.

Throughout the Middle and Late Holocene, the surface area of Saaremaa has been increasing, with smaller islands and shoals gradually emerging from the sea and merging with one another. The retreating ice sheet left behind extensive deposits of morainic and glaciofluvial sediments, which were subsequently reshaped by wave action, currents, and wind, giving rise to various accretional landforms (Raukas 2000). The Järve region (Fig. 1) is characterised by a sequence of elevated accretional palaeospits (Fig. 2), primarily composed

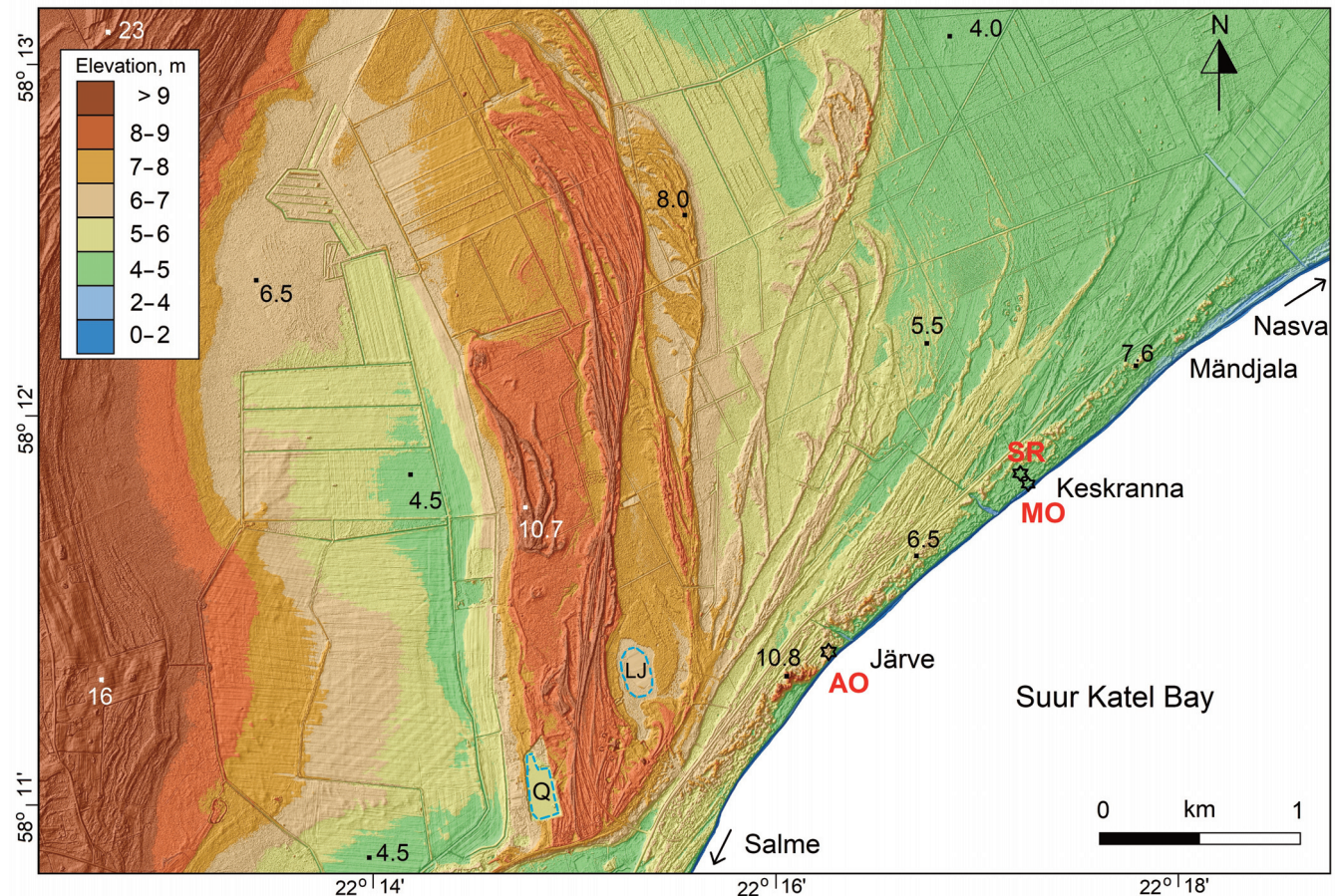

Fig. 2. LiDAR-based digital elevation model of the Järve study area (a few elevation marks are added). Locations of fieldwork: MO – master outcrop, SR – scarp rim, AO – additional outcrop; GPR profiles run between the MO and SR. LJ – Lake Järve, Q – quarry. Elevation at the main blowout near the AO is 10.8 m relative to the EH2000 datum. Arrows point towards the Salme and Nasva locations.

of marine sands interspersed with thin gravel layers, reaching heights of 10–11 m above present sea level (Luik et al. 2025). The Järve study area, located ~10–15 km west-southwest of Kuressaare, the island's largest town, borders a shallow bay in the Gulf of Riga known as Suur Katel. Coastal waters here are relatively shallow, with depths of less than 5 m extending 2–3 km from the shoreline. The area features a sandy beach, ~20–30 m wide, backed by sandy ridges and foredunes stretching ~8 km in length. The seaward ridge is predominantly 4–5 m high, with its highest point reaching 10.8 m above sea level at a blowout (Fig. 2). At Järve, wave action has eroded a scarp into earlier coastal sediments.

Although south-westerly and westerly winds dominate in Estonia, with an average wind speed in Saaremaa of ~6 m/s (Tarand et al. 2013), the Järve coast is currently predominantly influenced by winds and waves approaching from the south, and to a lesser degree from the southwest or southeast. Winds from the west–northwest–north–northeast sector, which is sheltered by land, practically do not excite waves at Järve. Due to the shallowness of the Suur Katel Bay and relatively short fetch distances (50 km to the south; the potentially up to 150 km fetch to the southeast is considerably hindered by Abruka Island), the long-term mean significant wave height near Järve is less than 0.4 m, and the maximum is up to 1 m (Najafzadeh et al. 2024). Hence, the Järve coast is a relatively well-sheltered, tideless, low-energy coast, where storm surges can occasionally reach heights of up to 1.6 m during extreme winter storms, such as the cyclone Gudrun on 9–10 January 2005 (Suursaar et al. 2006). The long-term annual mean temperature at the meteorological station in Sõrve (Fig. 1) is 7.5 °C, and it has increased by 0.037 degrees per year between 1951 and 2020 (Tõnisson et al. 2024a). The long-term average annual precipitation is ~590 mm, which slightly exceeds potential evaporation. Consequently, the foredunes and beach ridges become vegetated relatively fast, which is also favoured by relatively modest amounts of shifting sands. Due to the warming climate, the duration of both snow and ice cover has considerably declined in the area over the past seventy years. One consequence of this is that, particularly in winter, wave and hydrodynamic loads on the coastal zone have increased (Najafzadeh and Soomere 2024; Suursaar et al. 2025). Secondly, coastal sediment tends to persist for a shorter period in a frozen and more solid state (Tõnisson et al. 2024a).

The development of the Järve shoal, which soon evolved into an island, began ~4000 years ago. As the sea level fell, sediments from the emerging sea floor were reworked by waves from various directions into beach ridges and spits (Luik et al. 2025). About 3000 years ago, the expanding spit system had connected with Saaremaa. The gradual emergence of the Sõrve Peninsula and the ultimate closure of the Salme Strait (Nirgi et al. 2022) sheltered the Järve area from westerly wind and wave forcing. Sediment accumulation gradually shifted eastward, infilling shallow marine areas at Mändjala and extending the coastal barrier, which contributed to the isolation of the Mullutu-Suurlaht Lagoon by ~1600 CE (Suursaar et al. 2024). At the same time, intensification of dune formation occurred, likely influenced by the Little Ice Age

(LIA; usually considered to be between 1300 and 1850 CE) and anthropogenic factors such as deforestation (Jackson et al. 2019; Tõnisson et al. 2020; Luik et al. 2025). However, since the end of the LIA, rising air temperatures, reduced seasonal ice cover, and accelerating global sea-level rise have increasingly affected coastal processes (Tõnisson et al. 2024a). Although the Järve area is still undergoing postglacial isostatic rebound, with current geocentric uplift rates estimated at 2–2.3 mm/a (Suursaar and Kall 2018; Vestøl et al. 2019), this is compensated for, and even exceeded by, the ongoing sea-level rise (Luik et al. 2024a). Local relative sea-level (RSL) rise has caused a shift towards sediment deficit at Järve, as there is insufficient sediment being supplied from the nearshore sea bottom. However, during extreme storms, such as those in 1990, 1999, 2005, and 2007, the scarp erodes at rates of ~1–5 m per event, and the released sediment is transported eastward towards Mändjala and Nasva Port (Tõnisson et al. 2008; Suuroja et al. 2020; Luik et al. 2025). For a while, the cleaned-up scarp reveals some darker, gravelly streaks. Afterwards, the sandy scarp usually becomes levelled until the next erosion event forces it to steepen and migrate landward again (Tõnisson et al. 2024a).

2.2. Fieldwork, sedimentological analysis and chronology

This study builds upon fieldwork conducted between the 1990s and 2024, the results of which were partially presented in an earlier publication (Luik et al. 2025) and a data repository (Luik et al. 2024b). In this study, we present new results specifically focused on describing the Järve scarp, including new luminescence and radiocarbon dates obtained in December 2024 (Fig. 3). Another main aim was to document the apparent streaks in the scarp (Fig. 4) and to relate them to the development stages of the Järve coast and to varying forcings.

Fieldwork at the study site (Figs 2 and 3; 58° 11′ 53″ N, 22° 17′ 14″ E) was conducted on 4–5 December 2024. During excavation, the scarp talus was cleared of debris, and a near-vertical outcrop was exposed at elevations ranging from ~0.8 m to 3.6 m (in the EH2000 height system, relative to the Normaal Amsterdams Peil). The outcrop's lithology was described visually on-site, with sediment structure and grain size determined according to the Udden–Wentworth grade scale. The stratigraphic sequence was documented by measuring the thickness of each layer and recording the absolute elevation of stratigraphic boundaries and surfaces using a Leica GS09 RTK-GPS.

A total of 16 sand samples were collected for subsequent granulometric analysis in the laboratory using a Fritsch Analysette 3 PRO sieving apparatus. Before processing, the samples were dried at 60 °C. A set of standard mesh sizes (2000, 1000, 500, 250, 125, 63, and 36 μm) was used for fraction separation. After weighing and calculating the weight percentages of each fraction, statistical grain-size parameters were determined using the arithmetic method of moments in the GRADISTAT 8.0 software (Blott and Pye 2001).

An additional outcrop (AO in Fig. 2; 58° 11′ 25″ N, 22° 16′ 16″ E), located ~1.2 km southwest of the master

Fig. 3. Setting of the master outcrop (the sea-facing profile, marked with a red dashed line, is partly obscured); GPR instrument shown on the left. Fallen trees in the background indicate recent scarp erosion. Photo by Ü. Suursaar, 4 December 2024.
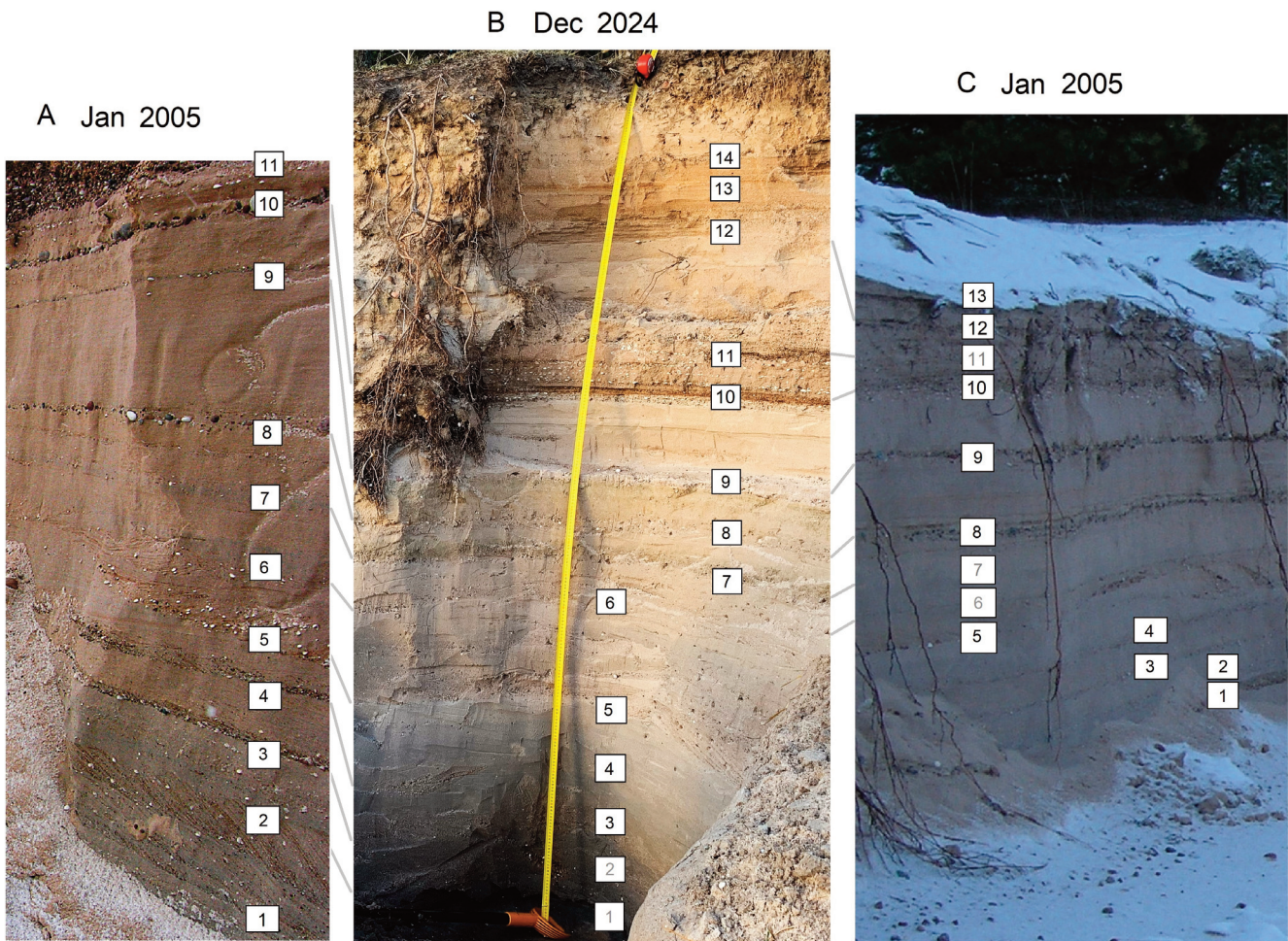

Fig. 4. Correlation of the storm or regime shift streaks (interbeds) on photos taken on 25 January 2005 (A, C; two different locations near the master outcrop, exact locations unknown) and on 4 December 2024 (B). Photos by K. Orviku (A), Ü. Suursaar (B), and H. Tõnisson (C).

Table 1. Radiocarbon (^{14}C) and luminescence (OSL) samples taken at the Järve scarp area. SE – sample elevations in the EH2000 system. Short codes R1* and L1* correspond to R1 and L1 in Luik et al. (2025)

Type	Code	Lab code	SE, m	Material	Reference
MO – master outcrop (58°11'53" N, 22°17'14" E)					
[14]C	C1	FTMC-XK54-1	0.80	Shells	This study
[14]C	C2	FTMC-XK54-2	1.69	Shells	This study
[14]C	C3	FTMC-XK54-3	2.05	Shells	This study
[14]C	C4	FTMC-XK54-4	2.45	Shells	This study
[14]C	C5	FTMC-XK54-5	2.90	Shells	This study
OSL	L1	25003Q	1.78	Sand	This study
OSL	L2	25004Q	2.31	Sand	This study
SR – master outcrop scarp rim (58°11'56" N, 22°17'11" E)					
[14]C	R1*	Poz-114329	4.01	Charcoal	Luik et al. (2025)
OSL	L1*	SJ15-OSL1	3.01	Sand	Luik et al. (2025)
AO – additional outcrop (58°11'25" N, 22°16'16" E)					
[14]C	C6	FTMC-HC21-2	5.35	Charcoal	This study
OSL	L3	25001Q	5.13	Sand	This study
OSL	L4	25002Q	5.57	Sand	This study

outcrop (MO), was partially cleaned and examined. From this secondary exposure, one radiocarbon and two OSL samples were collected. In total, four samples for luminescence dating were collected from sand deposits at the two outcrops (Table 1) using opaque PVC tubes (30 cm in length, 5 cm in diameter), which were inserted horizontally into the outcrop. Sampling depths were chosen to capture the point at which sand grains were likely no longer exposed to direct sunlight. Once extracted, the tube ends were sealed with duct tape and stored in darkness until analysis.

The luminescence analyses were conducted at the Lund Luminescence Laboratory, Lund University, Sweden. Sample preparation included sieving, treatment with 10% HCl, 10% H_2O_2, 10% and 40% HF, and density separation at 2.62 and 2.58 g/cm^3 (LST Fastfloat; Murray et al. 2021). Small (2 mm) single aliquots of quartz and K-feldspar grains were analysed in Risø TL/OSL readers, model DA-20, using single aliquot regeneration (SAR) protocols. Post-IR blue stimulation with 220 °C pre-heat and 180 °C cut-heat temperatures was used for quartz (Murray and Wintle 2000, 2003; Roberts and Wintle 2001), and a post-IR$_{50}$IR$_{225}$ protocol was used for K-feldspar (Buylaert et al. 2009). Doses were calculated using the Risø Analyst 4.57 software with exponential curve fitting; the first 0.48 s of the signal were integrated for the peak, and the last 4 s for background. Aliquots with a recycling ratio within 10% of unity, a test dose error <10%, and a relative dose error <30% were accepted. Sediment dose rates were determined with a dual α/β scintillator μDose instrument (Tudyka et al. 2018), and total environmental dose rates and ages were calculated using the DRAC online calculator v1.2 (Durcan et al. 2015). Average water content was assumed to be similar to or slightly higher than that at the time of sampling. Ages were calculated based on the mean dose and the central age model (CAM; Galbraith et al. 1999) using the function calc_CentralDose v.1.4.1 (Kreutzer et al. 2025).

For comparison and verification of the dates, five seashell samples were taken from the MO and one charcoal sample from the AO (see Fig. 5A; Table 1) for radiocarbon dating. The analyses were conducted at the Vilnius Radiocarbon Laboratory, Lithuania, using a single-stage accelerator mass spectrometer (SSAMS; NEC, USA) and automated graphitisation equipment AGE-3 (Ionplus AG, Switzerland). Following chemical preparation, the samples were treated with phosphoric acid and subsequently graphitised. Reference materials IAEA C2, SIRI K, and NIST-OXII were used throughout the process. The calculated ^{14}C ages were calibrated into calendar years using the IntCal20 calibration curve (Reimer et al. 2020) in the OxCal v.4 online software, and presented alongside with their 68.3% probability limits. Table 1 also includes two earlier samples taken from the scarp rim (SR in Fig. 2), located a few dozen metres inland from the MO, previously presented by Luik et al. (2025).

Providing additional data on layering in the deposits, two GPR profiles were taken along a 50 m transect across the scarp, ~10 m west of the outcrop, and parallel to the scarp on top of its rim. The two GPR profiles cross each other ~15 m northwest from the outcrop (roughly between the MO and SR; Fig. 2) at 58° 11′ 53″ N, 22° 17′ 13″ E. An ImpulseRadar (model CO730) was used with transceivers operating at 70 and 300 MHz, featuring ranges up to 400 ns and a trace spacing of 0.02 m (for details, see Muru et al. 2018). The digital GPR data were post-processed and visualised using GPR-SLICE software.

To assess heavy mineral concentration (HMC) in sand sediments, vertical profiles of low-field magnetic susceptibility (MS) were determined using two devices. Twenty-nine samples were collected across the entire profile at 10 cm intervals and later analysed in the laboratory for MS using a Bartington MS3 meter with MS2K surface scanning sensor (Pupienis et al. 2017). The measurements were performed at constant room air temperature; each sample was measured three times, and the final MS value represents the average of three readings. After every nine measurements, the instrument was reset and calibrated using a calibration sample provided
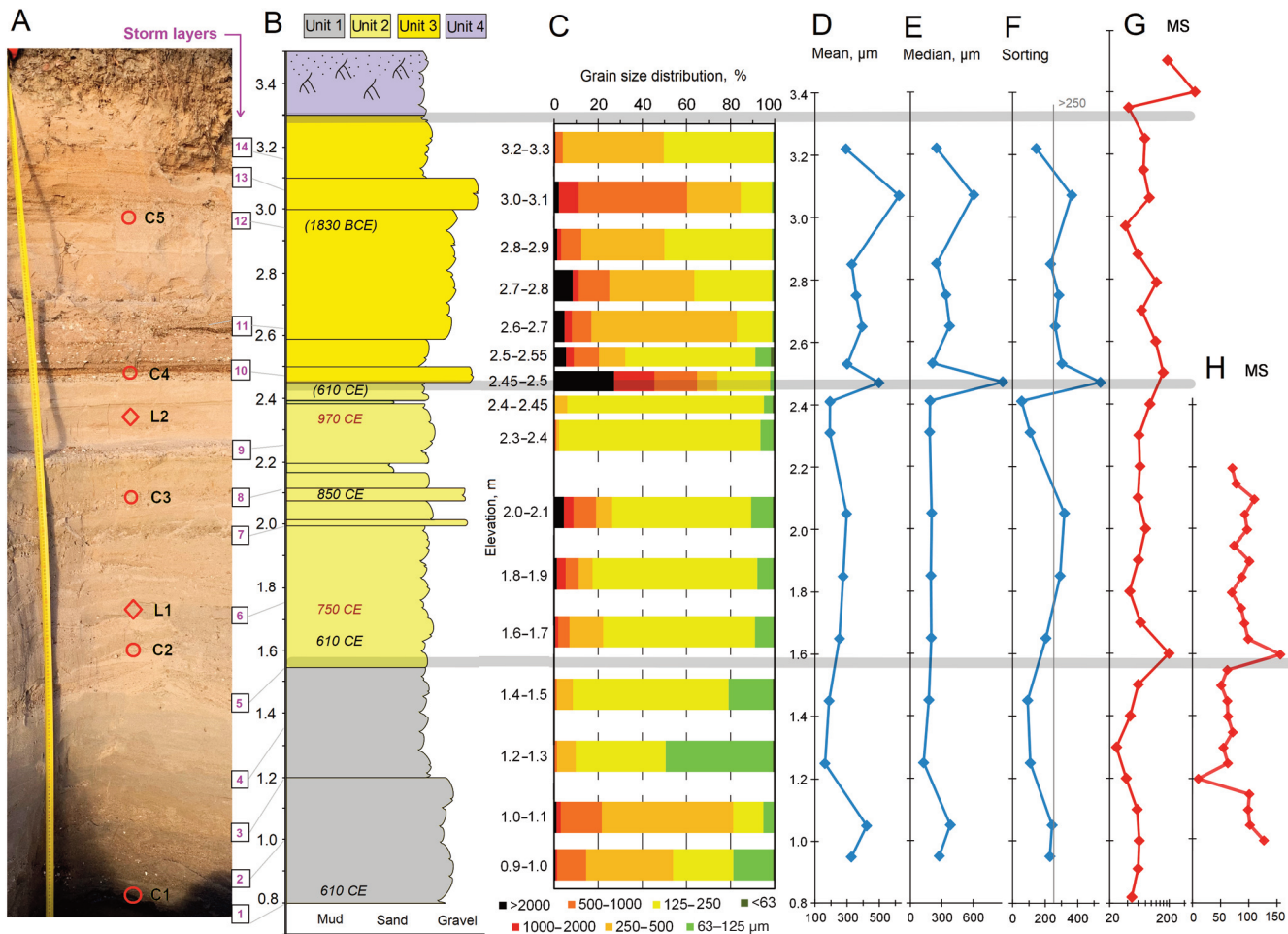
Fig. 5. Photo of the Järve outcrop (A) showing the locations of radiocarbon (C1–C5) and OSL (L1, L2) dates, as well as enumerated inter-beds or storm layers (1–14; see also Fig. 4). Note that the vertical scale varies slightly in the slant photo (A). Sediment stratigraphy (B) and granulometry (C–F) of the Järve scarp are based on sand sample analyses. The boundaries of the sedimentary units (1–4) are marked with thick grey lines. The obtained dates are shown in B; the radiocarbon ages C4–C5 are not reliable (see Discussion) and therefore appear in parentheses. Magnetic susceptibility (MS, values in 10^{-6} SI units) is presented in G and H (log scale in G). Photo by Ü. Suursaar, 4 December 2024.

by the manufacturer (Dearing 1999). Bulk MS serves as a reliable indicator of allochthonous mineral matter in sediments and thus probable storm layers (Pupienis et al. 2017; Buynevich et al. 2023). Measurements were also taken on-site using a magnetic susceptibility meter SM-30 (ZH instruments, Czech Republic). Readings were taken every 5 cm in the lower half of the pit, at elevations ranging from 1 to 2.2 m (in EH2000).

2.3. Auxiliary elevation and forcing data

The general evolution of the study area has been previously analysed in our recent article (Luik et al. 2025). In the present study, we narrow our focus to the development of the Järve scarp along the current erosional section, which spans ~2–3 km along the shore. To establish the background setting, a digital elevation model (DEM) was constructed utilising LiDAR elevation data provided by the Estonian Land Board (ELB 2025b; Fig. 2). The elevations are given in the EH2000 system. Through cartographic analysis using GIS, we examined the present-day landforms – such as individual beach ridges and spits, erosional scarps, and the beach face – and evaluated changes in the coastline linked to various forcing factors.

Historical maps (ELB 2025c) and field photos taken at various times (1990, 2004, 2005, and 2024; ELB 2025d) were compared. In discussing our results, we considered data partially presented in the data repository (Luik et al. 2024b), as well as findings from our previous studies on Late Holocene relative sea-level changes (Nirgi et al. 2022; Suursaar et al. 2024), potential shifts in wind and storm regimes (Suursaar et al. 2015; Suursaar 2023; Tõnisson et al. 2024a), ice conditions (Suursaar et al. 2025), and sediment dynamics over recent decades (Orviku 2006; Suuroja et al. 2020; Luik et al. 2025).

3. Results and interpretation

3.1. Lithological description of the sediments in the Järve outcrop

During the fieldwork, the water line was ~10 m seaward from the exposed outcrop. The base of the outcrop was at an elevation of 0.8 m, and its cleaned-up top reached 3.6 m in the EH2000 system. No long-term sea-level measurements exist for Järve, but based on interpolated statistics from nearby coastal stations (mainly Pärnu and Ristna; Fig. 1A), the current mean sea-level height in this area is around zero in the (old) BK77 system, or 0.2 m in the EH2000 system

(Tõnisson et al. 2024a). As a result of southerly winds (5–8 m/s), the sea level varied between 0.2 and 0.4 m on 4–5 December 2024 (EWS 2025). Several fallen tree trunks in the surrounding area indicated erosion events during previous winter storms (Fig. 3). At the scarp, the groundwater table was recorded at 0.8 m.

The visual assessment of the outcrop revealed that the deposits consisted predominantly of sand with some gravel and very little silt. There were some darker layers (interbeds) consisting of coarser sand fractions and seashells (Figs 4 and 5). When juxtaposing the outcrop photo with older photos taken roughly from the same location, the patterns of inter-beds appeared partly similar. We identified and correlated 14 interbeds (Fig. 4), which were provisionally called 'storm layers'. Although layers 1–14 should be the same in all pho-tos, the darkness and thickness varied somewhat, probably due to differences in moisture conditions and the natural variability of the layers. Some were darker layers with coarser material (e.g. 10 and 11 in Fig. 4), whereas others appeared as erosional surfaces between cross-bedded and laminated layers; these layer indicators were drawn just above the erosional surface (e.g. 2 and 5 in Fig. 4).

According to granulometric analysis (Fig. 5C–F), the sediment was sandy in all layers. It was mostly moderately or poorly sorted, as the threshold for well-sorted sediment was approximately < 90–110 μm, and > 230–360 μm for poorly sorted sediment (Fig. 5F). Seashell fragments occasionally occurred throughout most of the outcrop and were sometimes abundant, e.g. between layers 10 and 11 (Fig. 4). Based on lithological and structural characteristics, the entire sequence can be divided into four main sedimentary units (Fig. 5B). In general, longshore transport prevailed in units 1 and 2, cross-shore transport in unit 3, and aeolian input in unit 4.

Unit 1 (elevation from 0.8 to 1.55 m, ~75 cm thick; Fig. 5) consisted of greyish-beige medium- to fine-sand beds (layers), for which four granulometric analyses were performed. The two lowermost beds were cross-laminated (with shore-parallel dip), composed primarily of poorly to moderately sorted me-dium sand with interlaced dark mineral laminae, occasional shells, and gravel grains. Mean grain size reached 422 μm and median 359 μm in the 1.0–1.1 m sample (Fig. 5C–E). The two upper beds in this interval were horizontally lami-nated, consisting of well-sorted very fine to fine sands with occasional shell fragments. The lowest mean (163 μm) and median (126 μm) grain-size values of the entire profile were found there. The lower boundaries of these beds were sharply marked by ~10 cm thick layers of coarser sand and gravelly sand, possibly representing storm deposits.

Unit 2 (1.55–2.45 m, 90 cm thick; Fig. 5) consisted of beige medium- to fine-sand beds, from which five granulometric samples were collected. Moderately to poorly sorted fine sands dominated. The two lowermost beds in this unit were high-angle cross-laminated (up to 29° towards east–northeast, i.e. shore-parallel) fine to medium sands. In the middle (2.0–2.1 m), a poorly sorted fine-sand layer with a multi-modal distribution consisting of 10.2% coarse sand was found. The three upper beds were horizontally laminated, composed of fine sand, with organic laminae present at 2.2 and 2.4 m. The lower boundaries of these beds were also defined by coarser deposits (6–10 cm thick), forming an erosional base and interpreted as storm deposits.

Unit 3 (2.45–3.3 m, 85 cm thick; Figs 5 and 6A) comprised subhorizontally laminated sand beds that contained five sandy–gravelly sub-layers, interpreted as storm deposits. The beds consisted of fine to medium sand that was reddish brown to beige and subhorizontally laminated. The lower boundaries of these beds were marked by layers of coarse sand and gravelly sand deposits (1–5 cm thick). Four to five shell layers between 2.4 and 2.6 m (Fig. 5) were present in the basal part. Shells were exceptionally well preserved and occurred in distinct, continuous layers. Seven granulometric samples were analysed. In general, the samples contained larger proportions of coarse fractions and were poorly sorted. The sample immediately above the lower unit (at ~2.5 m) was poorly sorted very coarse sand with a trimodal, skewed distribution, with a mean of 499 μm and a median of 846 μm. It included 19.4% of coarse sand. On top of this layer, several strata of poorly sorted fine to medium sands occurred, with occasional shells.

Unit 4 (3.30–3.50 m, ~20 cm thick; Fig. 5) comprised massive fine- to medium-grained light brown humus-rich sand with roots and pebbles. The sand in this unit was likely modified by aeolian and paedogenic processes. Aeolian influence was weak at this location, but the thickness of the
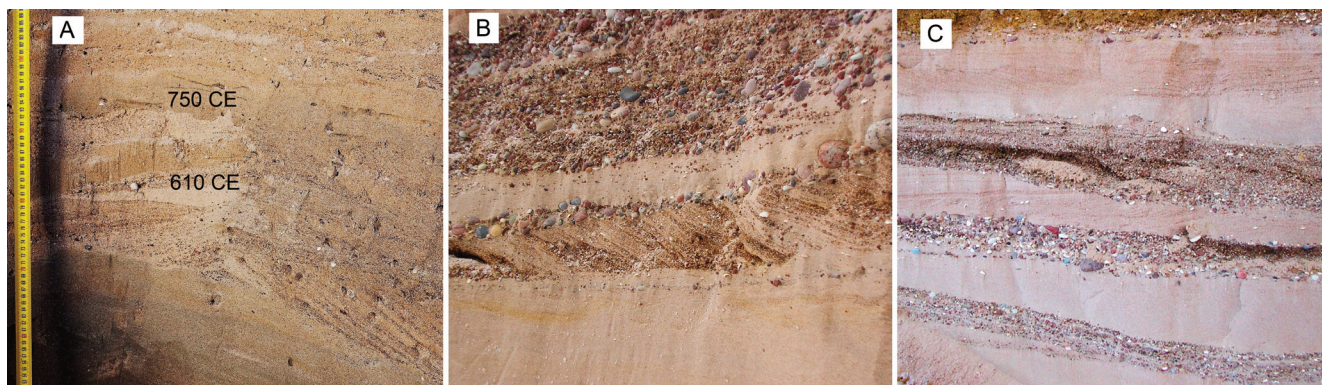

Fig. 6. Close-up views of cross-bedding at the Järve scarp from 4 December 2024 (A; elevation ~1.4–2.0 m) and from 25 January 2005 (B, C; close to the land surface at ~3.5–4 m, although the exact elevation, scale, and location are unknown). Dates were available for A (see Fig. 5) but not for B and C. Photos by Ü. Suursaar (A) and K. Orviku (B, C).
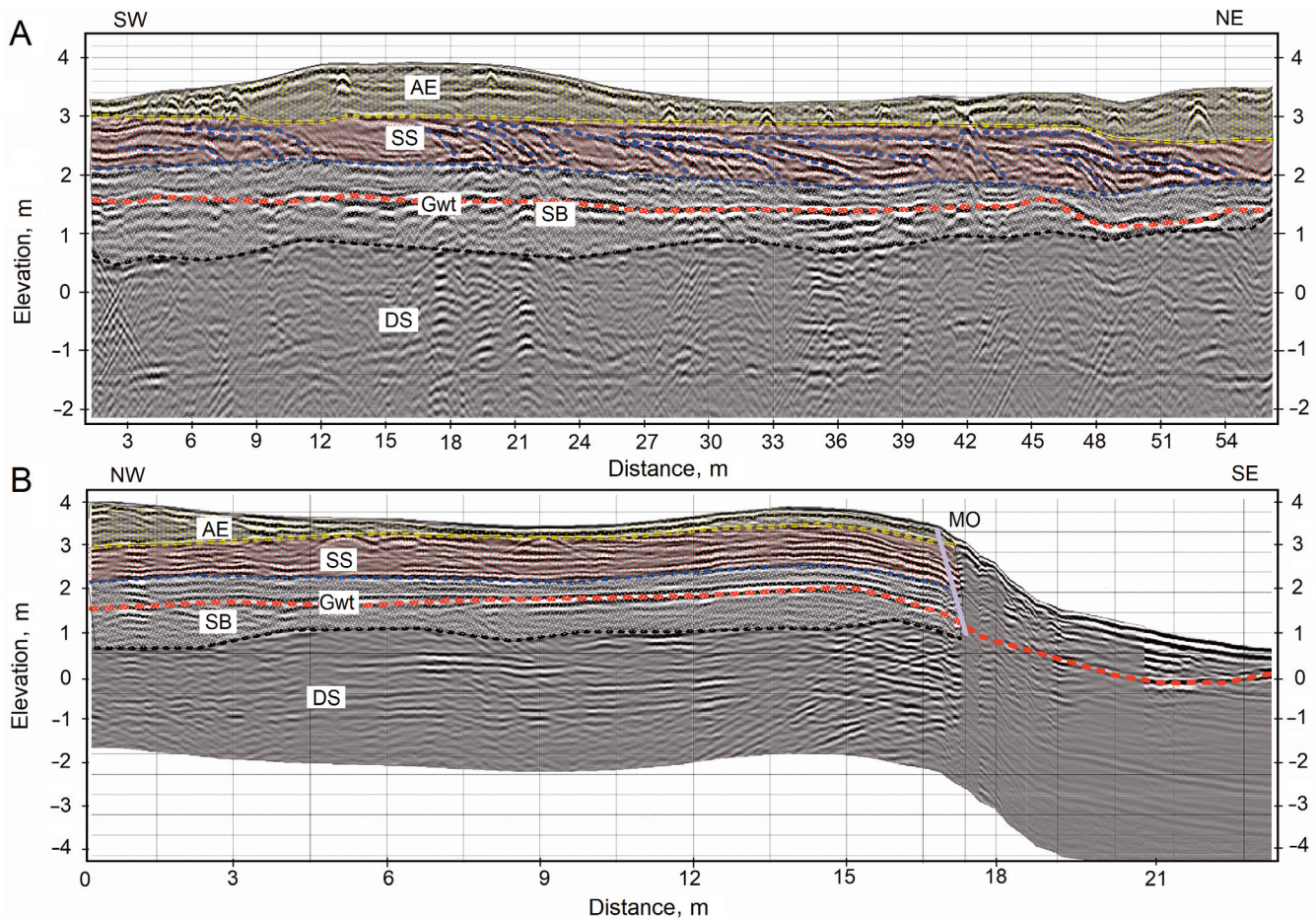
Fig. 7. GPR profile fragments taken alongshore (A) and cross-shore (B) in December 2024. Note that layering is unreadable in the steep outcrop section (B). AE – aeolian facies (sand); SS – spit sediment (sand with gravel and pebbles, wave-transported, longshore-dipping increments); SB – underwater nearshore sandbar (cross-bedded); DS – deeper sea/glaciofluvial sediment (reworked from submerged glaciofluvial sand and clayey moraine deposits); Gwt – groundwater table (red dashed line); MO – master outcrop, the cleaned scarp. Parabolic features visible at elevations ~3 m (horizontal distance 3–9 m in A) are artefacts. The profiles cross each other at ~20 m (A) and ~2 m (B).

aeolian layer varied between 0–1 m in the very proximity of the outcrop and reached up to ~5 m (at the 10.8 m absolute elevation mark; Fig. 2) at the blowout site 1.5 km to the southwest.

The MS values (Fig. 5G, H) showed higher values in the lower part of the pit (0.8–1.0 m), at the lower boundary of unit 2 (around 1.6 and 2.5 m), and in the upper zone affected by paedogenic processes (unit 4). Smaller maxima were also found at around 2.0, 2.8, and 3.1 m (note the logarithmic scale in Fig. 5G). Most of these maxima coincided with the enumerated (1–14) storm (or regime-shift) layers, though not universally because some interbeds included only some strata of coarser fractions without erosional surfaces.

The GPR profiles obtained at the MO location also showed some distinct layering (Fig. 7). In general, facies of sub-horizontally layered sea-bottom sediment (DS), marine-built underwater sandbar (SB) and spit sediment (SS), and aeolian deposits (AE) can be identified (Fig. 7). The slant layers in the SS facies indicated spit elongation, where each stronger storm or stormy season likely resulted in a new tongue-like increment. These longshore-dipping reflectors (visible in Fig. 7A) were not well differentiated on the cross-shore profile (Fig. 7B). Due to the inherent vertical resolution (~20 cm) of the GPR imagery, the sub-parallel streaks

(between 2–4 m in Fig. 7B) cannot be individually correlated with the streaks visible in Fig. 4. Moreover, some of the streaks in Fig. 4 showed only insignificant granulometric differences and therefore did not necessarily create a reflector on the GPR image. Several reflectors occurred in the DSs around –1.5 m (Fig. 7A), likely originating from gravelly sublayers or lenses within the older buried valley. Some appeared only as discontinuous or short reflectors. This glaciofluvial-type sediment is also observed, for example, in the Quaternary cover maps (ELB 2025a) and in the quarry near Lake Järve (Fig. 2). The groundwater table undulated around 1.5 m in the interior of the spit; it descended steeply in the scarp area (0.8 m) and reached zero near the shoreline. In general, the layers were undulated (by up to 1 m) in height, which also explains the variations and differences in layers visible in Fig. 4. It is also important to note that over the past 19 years, the scarp has receded by ~5 m at that location (Luik et al. 2024a), hence the layers cannot lie in exactly the same positions as in Fig. 4A and B. Nevertheless, the layered, varying nature of the outcrop is obvious (Figs 4, 5 and 7).

3.2. OSL and ^{14}C dates

Though the luminescence signal from the quartz was relatively weak, it had a strong or dominant fast component, and

the excellent dose-recovery ratio (1.00 ± 0.04, n = 19) showed that the analytical protocols can accurately recover a given dose. Only a few aliquots of K-feldspar were measured, and due to relatively high residual doses (0.4–7.6 Gy) compared with the equivalent doses (1.9–8.8 Gy), as well as fading, the quartz ages (Table 2) were preferred for age determination. Additional information on quartz and feldspar analyses (not used in the article) is provided in the Supplementary material (Tables S1–S3).

The ages obtained from the middle part of the MO, 53 cm apart, differed by ~220 years (970 CE and 750 CE; Table 2). In the AO, near the blowout, although samples L3 and L4 were vertically only 44 cm apart (depths of ~1.1 and 0.7 m from the outcrop rim; Fig. 8), their ages differed considerably. As in the MO, the lower dating clearly corresponded to the original landward ridge, built entirely by the sea. The upper sample was probably formed at a later stage by a combination of aeolian and marine processes, when the ridge gained height and lateral width. The dark palaeosoil streak between these two samples marked a significant regime shift. The uppermost aeolian-facies age (1630 ± 310 CE; Table 2) corresponded to our earlier dates for the Järve dune. According to Luik et al. (2025), the radiocarbon sample R1* (Table 1) gave an age of 1460 ± 30 CE for the dune facies just behind the MO scarp, and an OSL sample (code L2b in Luik et al. 2025) yielded both U-pIRIR and pIRIR dates at ~1400 ± 100 CE.

In Table 3, calibrated years based on the IntCal20 curve are presented in three different versions. The first one (*R(0)*), which is valid for the charcoal sample C6, is not appropriate for the seashell samples C1–C5. It is well known that radiocarbon dating of seashells can be compromised by the so-called marine reservoir effect (e.g. Long et al. 2012). This effect is highly variable, and its exact values are not known for the Gulf of Riga. As an assumption, we rely on fig. 6 in Lougheed et al. (2013), which indicates that the effect may vary from about 400 radiocarbon years at the Danish Straits

to 25–50 years at the bottom of the Bothnian Bay. The study did not provide estimates for the interior of the Gulf of Riga, but the regression-based estimate for the Baltic Proper, near the West Estonian Archipelago, was 200–250 years. Decreasing alongside salinity from the open sea to the bay, this effect can be tentatively estimated at about 200 ^{14}C years in our study area. Therefore, for the second set of dates (*R(200)* in Table 3), 200 years were subtracted from the ^{14}C ages before calibration with IntCal20. In addition, the coastal sea south of Saaremaa is marked as a hard-water-prone area in Lougheed et al. (2013), which can add more than 500 ^{14}C years to the correction (*R(t)*). Silurian limestone is widespread on Saaremaa and occasionally outcrops along coasts and streams. The hard-water correction was determined empirically by comparing OSL ages with ^{14}C dates (Tables 2 and 3). Consequently, the third set of dates is presented in Table 3, with the total correction applied (200 + 500 = 700 years).

Fig. 8. Locations and ages of two luminescence dates (L3, L4; grey sampling tube ends visible in the outcrop) and one ^{14}C date (C6) near the blowout (AO in Fig. 2; Table 2). Photo by Ü. Suursaar, 5 December 2024.

Table 2. Luminescence (quartz) dates from the master outcrop (L1, L2; Table 1; Fig. 5) and the additional outcrop (L3, L4; Fig. 8). SE – sample elevation; WC – sample water content; CAM – Central Age Model (weighted mean) age (ka = 1000 years); MD – mean dose; n – number of aliquots

Code	Lab code Lund	SE, m	WC, %	CAM age, ka	MD, Gy	n, accepted/total	Dose rate, Gy/ka	Age, CE
L1	25003	1.78	12	1.28 ± 0.07	2.54 ± 0.07	27/48	1.98 ± 0.10	**750 ± 70**
L2	25004	2.31	8	1.06 ± 0.08	2.23 ± 0.11	23/39	2.06 ± 0.12	**970 ± 80**
L3	25001	5.13	8	1.44 ± 0.12	2.65 ± 0.16	17/24	1.86 ± 0.10	**590 ± 120**
L4	25002	5.57	8	0.39 ± 0.31	0.69 ± 0.05	21/48	1.78 ± 0.10	**1630 ± 310**

Table 3. Radiocarbon dates (^{14}C, years BP), calibrated years ((Min and Max at the 68.3% probability level), and median (Med); CE; –CE = BCE), presented in three different versions using IntCal20: no correction (*R(0)*), marine reservoir effect correction (*R(200)*; Lougheed et al. 2013), and empirical reservoir + hard-water correction (*R(700)*). SE – sample elevation

Code	SE	^{14}C	Lab code	R(0) Min	R(0) Max	R(0) Med	R(200) Min	R(200) Max	R(200) Med	R(700) Min	R(700) Max	R(700) Med
C1	0.80	2165 ± 29	FTMC-XK54-1	−360	−160	−210	10	120	60	580	640	610
C2	1.69	2162 ± 30	FTMC-XK54-2	−360	−150	−200	20	120	60	580	650	610
C3	2.05	1883 ± 30	FTMC-XK54-3	120	210	160	260	420	380	880	890	850
C4	2.45	2155 ± 30	FTMC-XK54-4	−350	−110	−190	20	120	70	590	650	610
C5	2.90	4215 ± 33	FTMC-XK54-5	−2900	−2700	−2790	−2580	−2470	−2530	−1900	−1770	−1830
C6	5.35	740 ± 28	FTMC-HC21-2	1260	1290	1270						

4. Discussion

4.1. Mismatch between OSL and ^{14}C dates; marine reservoir and hard-water effect

In comparison with the OSL samples, the radiocarbon samples, except for C6, appear to be offset to varying degrees (Tables 2 and 3). The uppermost two dates in the MO (C4 and C5) are older than those below (C1–C3) and are therefore highly questionable, but even the lower samples (C1–C3) remain problematic. In the non-corrected version (Table 3: *R(0)*), the offset from the OSL dates is ~900–1200 years. After applying the reservoir effect correction (Table 3: *R(200)*), the offset decreases to ~700–900 years. Finally, when applying both the reservoir and hard-water corrections (*R(700)*), the C1–C3 dates become comparable with the OSL ages (Table 4). By contrast, the charcoal sample (C6 from the AO), taken between OSL samples L3 and L4 (Table 3; Fig. 8), does not require any correction and aligns well with the OSL results (Table 4).

Unfortunately, the proper quantification of these effects is not well established, which considerably reduces the reliability of seashell-based dates. The marine reservoir effect arises because terrestrial organisms obtain ^{14}C directly from the atmosphere, whereas marine organisms, such as molluscs and fish, may incorporate older carbon from seawater (e.g. Long et al. 2012). As a result, radiocarbon ages are typically (i.e. globally) offset by ~400 years, but the magnitude of this effect is highly variable in space and time (Ascough et al. 2005; Alves et al. 2018). Several estimates exist for the Baltic Sea region. For example, Hedenström and Possnert (2001) reported variations ranging from ~750 years to near zero within a single sedimentary sequence from Lake Lilla Harsjön (an isostatically isolated basin in Sweden) spanning about 7000 years. In this study, the correction *R(200)* was adopted from fig. 6 in Lougheed et al. (2013). That study also indicated that the so-called hard-water effect can add more than 500 years to radiocarbon ages in areas underlain by limestone. The empirically estimated correction used here (Table 3) roughly corresponds to this suggestion by Lougheed et al. (2013). However, these corrections remain tentative and are not yet supported by direct on-site measurements.

A third effect is the possible relocation of seashells, meaning that they may not have died and been buried at their present location. This process can be even more variable than the effects mentioned above. It may occur on a relatively small scale through the displacement of shells during deposition in the coastal marine environment. For instance, a 200–250-year discrepancy in ages can arise from merely 50 cm vertical misplacement of shells. Freshly dead and unmineralised seashells contain voids and organic matter, making them less dense (~1 g/cm^3 or even less) than the surrounding sand (~2.7 g/cm^3). When sifted back and forth by waves on the shallow seabed near the coast, seashells can remain on the sediment surface for longer, while grains of sand settle downward. Storm waves can also toss clams and seashells onto the beach, forming so-called shell ridges. When buried under the sand, these shells are apparently 'older' than the surrounding sediment indicates. For example, if the shell ridges occur up to a metre above the usual waterline, this would mean a potential age difference of up to 450 years at 2.2 mm/a uplift.

However, for the upper two samples in the MO (C4 and C5), the obtained ages are ~1000–3500 years older than expected. The most plausible explanation is the reworking and relocation of previously buried material that was later eroded and redeposited. It is well established that the Järve palaeospit developed through sediment accretion and postglacial uplift over ~4000 years (Luik et al. 2025). After the closure of the Salme Strait, the alongshore supply of new sediment from the west diminished, and the Järve coast was increasingly subjected to erosion for various reasons.

It was not possible to determine the precise provenance of the shells in samples C4 and C5. Unlike luminescence samples, which are reset with each episode of bleaching and redeposition, radiocarbon ages reflect the time of death of the organism and not the location of redeposition. Consequently, the radiocarbon ages of C4 and C5 likely do not provide reliable information in the stratigraphic context of this study. Regrettably, shells were the only datable organic material available at the Järve MO.

It can be concluded that, unlike the charcoal-rich humic layer (the dark layer dated to 1270 CE in Fig. 8), seashells cannot be considered reliable dating material in coastal stratigraphic studies at accretional–erosional seacoasts (see also e.g. Long et al. 2012). Seashells are subject to reservoir and hard-water effects and may also be displaced by waves, deposited and eroded multiple times, transported alongshore, and ultimately redeposited in new locations. All these effects may be present at the Järve study site, but their separate roles cannot yet be estimated. To accurately determine these effects in the Gulf of Riga, further localised studies are necessary. These would require either paired terrestrial and marine samples from the same context or the parallel use of different dating methods.

Table 4. Vertical sequence (from lower to higher elevation) of luminescence and radiocarbon dates from the main outcrop (MO), additional outcrop (AO), and scarp rim (SR, codes R1* and L1*; Luik et al. 2025; Fig. 5A; Tables 1–3). The strongly offset age of the probably relocated sample C5 is discarded here; C4 is also questionable. SE – sample elevation; age includes reservoir and hard-water effect corrections in C1–C4); FE – formation elevation of deposits, calculated considering the present-day elevations (SE), the 2.2 mm/a uplift rate, and corrected ages

Location	Code	SE, m	Age, CE	FE, m
AO	L4	5.57	1630	4.7
AO	C6	5.35	1270	3.7
AO	L3	5.13	590	2.0
SR	R1*	4.01	1522	3.1
SR	L1*	3.01	620	0.0
MO	C4	2.45	610	–0.7
MO	L2	2.31	970	0.0
MO	C3	2.05	850	–0.5
MO	L1	1.78	750	–1.0
MO	C2	1.69	610	–1.5
MO	C1	0.80	610	–2.4

4.2. Possible provenance of the sub-layers in the outcrop

According to the stratigraphic and granulometric analyses (Figs 5 and 7) and the obtained or estimated dates (Table 4), the lowermost unit 1 was deposited in a shallow (–2.5…–1.5 m) nearshore sea ~1300–1500 years ago. The sediment consisted mostly of sub-horizontally laminated marine (Limnea Sea) sand (Suuroja et al. 2020; Tõnisson et al. 2022) and included a few strata of slightly coarser material, seashells, and cross-bedding. As a rule, sets of underwater sandbars developed along sandy shores in Estonia (e.g. Tõnisson et al. 2024a, 2024b, 2024c). Such sub-parallel ridges are also visible on aerophotos along the Järve–Mändjala coast, especially closer to Nasva Harbour (ELB 2025d; Luik et al. 2025). The relative height of underwater bars is ~0.5 m, and those situated closer to shoreline sometimes appear above the water surface in low sea-level conditions. The sediment in the lowermost part of the studied outcrop is not necessarily from the crest of the bar, but more likely from the trough (Fig. 7). However, the layers vary spatially and appear at slightly different elevations as the scarp retreats. On emerging coasts, underwater bars quite often (but not necessarily always) form a core for future beach or foredune ridges.

Unit 2, between present-day elevations of 1.55 and 2.45 m, is also of marine origin and likely formed just below or close to the water surface (–1.0…0.0 m; Table 4) ~1300–1100 years ago, whereas unit 3 (the layer between 2.45 and 3.3 m), judging by its elevation and internal layered structure (Fig. 7A), formed above the sea surface. The ridges grew both lengthwise and sideways, subsequently merging into larger spits. The lengthwise elongation of the spit is also traceable on the GPR image (Fig. 7A). Unit 2 includes several cross-bedded zones that indicate storms arriving from different directions (i.e. basically either southwest or southeast) and varying hydrodynamic regimes. Sediments of units 2 and 3 (Figs 5 and 6) also exhibit distinct layers of coarser material (due to combined cross-shore and longshore transport), which must have been eroded by storm waves from the nearby sea bottom and tossed onto the shoreface. Since the Salme palaeostrait between Saaremaa and Sõrve (Figs 1B and 2) must have been practically closed by that time (Nirgi et al. 2022), no additional material from the hydrodynamically more energetic Baltic Proper side (Najafzadeh et al. 2024) could have entered the Suur Katel Bay from the west.

Unfortunately, the sediments of the layers of units 3 and 4 in the MO remain without direct dating results so far. Still, considering the stratigraphy and granulometry (sub-layers of coarse sand; some cobbles and seashells; Fig. 5), the sediments of unit 3 were likely formed by a combination of marine and aeolian processes and deposited before the onset of dominant aeolian activity (unit 4) during the LIA. Considering the 2.2 mm/a uplift rate, unit 3 (2.45–3.3 m layer in the MO) is probably 700–1000 years old. On top of that, the aeolian layer (unit 4) is very thin and intertwined with paedogenic processes. Considering the present-day elevation, the material cannot be younger than the dune (1400–1600 CE; Luik et al. 2025). A previously obtained radiocarbon age from approximately the same location, but 20–25 m inland and closer to the land surface, was ~1450 CE (Luik et al. 2025). This indicates that, before the recent erosion stage began, beach ridges (spits) gradually grew seaward, with older ones located inland and younger ones closer to the sea. Due to the relatively humid climate and moderate wind conditions, foredunes and beach ridges normally become fixed by vegetation relatively fast in Estonia (e.g. Ratas et al. 2011; Vilumaa et al. 2017; Suursaar et al. 2022). However, the younger marine-built ridges are now missing (eroded away) on the seaside, which makes it impossible to obtain the corresponding dates in the scarp. Although the dune part is also missing in the upper part of the present-day outcrop, the 0.2–1.0 m thick (and 400–600 years old) aeolian cover reappears the score of metres inland (Fig. 7B) and also occurs in the AO (Fig. 8; Table 4).

The sporadic aeolian layer is essentially composed of reworked spit sand that has been reblown from its initial elevation of 2–4 to 6–10 m. After the dune formed, it began to roll landward, gradually feeding on itself. Today, only the younger part of this dune has survived, as material from the 'older' (original) part of the dune has either been blown landward or eroded away from the seaward side.

4.3. Development stages, shifts, and storm layers over the past 2000 years

Currently, the most seaward part of the Järve palaeospit, where the studied scarp is located, likely emerged from the sea ~1400–1600 years ago (Luik et al. 2025). It grew in height and volume through both sediment accretion and post-glacial uplift (amounting to ~3.5 m in height over the past 1600 years). As revealed by the granulometric–stratigraphic analysis, the lower part (nowadays 0.8–1.4 m) of the examined outcrop was formed by accumulation on the shallow nearshore sea bottom, possibly on top of the underwater bar (Fig. 9A). The shore-parallel, cross-bedded laminae indicate rapid spit growth both in width and length towards Mändjala (Fig. 9B). Several darker (coarser) streaks and variations between different lamination regimes indicate changes in forcing conditions (i.e. storminess) and sediment provenance.

The 14 identified streaks (interbeds or storm layers; Fig. 4) occur between 0.8 and 3.2 m and correspond to ages from 610 CE (Table 4) to ~1300 CE, yielding on average a period of ~50 years per stripe. The distances between the streaks are uneven. Between C1 and L2 (Table 4), for instance, there are nine streaks covering ages between 610 and 970 CE. A roughly 50-year periodicity suggests that the interbeds formed during exceptionally strong storms (e.g. storms such as those in 1967 and 2005), which were capable of accreting material that differed from routinely accumulated material – either coarser fractions or darker material with higher heavy-mineral content and MS values (Buynevich et al. 2023, 2024). In that sense, interbed 10 (Fig. 5) prominently features both in granulometry and MS values. Its formation time was ~1000–1100 CE (Table 4). The interface between units 1 and 2 (events between 610 and 790 CE) and the layer around interbeds 2 and 3 in the lower part of
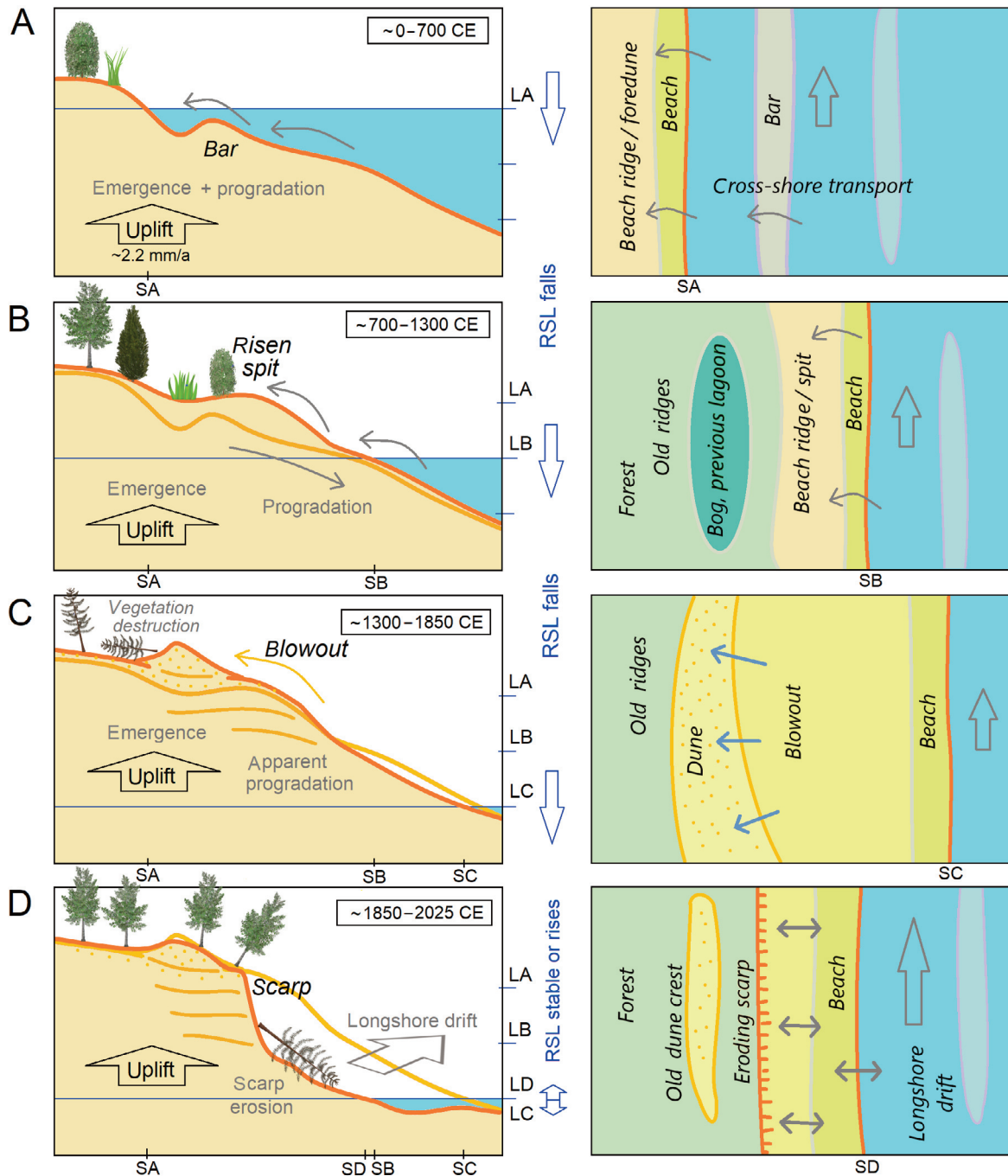
Fig. 9. Conceptual model illustrating the developmental phases of the Järve coast over the past ~2000 years, shown as cross-sections (left panel) and views from above (right panel). Emergence of a spit due to uplift and initial beach ridge accumulation followed by stabilisation by vegetation (A–B); activation of aeolian processes due to vegetation destruction and/or the colder climate of the LIA (C); and activation of coastal erosion due to relative sea-level stabilisation or rise, cessation of fresh marine sediment accumulation at Järve, and increasing storm impacts during ice-free winter conditions (D). SA–SD denote shoreline positions in stages A–D, and LA–LD denote sea levels in stages A–D. In the left panel, the orange line represents an incremental change compared to the yellow line representing the previous stage. A few storm layers are indicated (in C and D).

unit 1 (610 CE) are also more distinct. Some interbeds were probably not exactly accretional storm layers but erosional surfaces between cross-bedded and laminated layers (i.e. evidence of storm erosion) or just marked particular periods in the gradual accumulation process under varying sedimentary conditions. Because these former underwater formations – although buried – are now elevated above sea level, we can study storminess shifts in the Järve scarp through these formations. This is rarely feasible elsewhere, as comparable work typically requires underwater sampling.

An obvious shift in the development of the raised Järve coast was the onset of LIA dune formation (Fig. 9C). This process has been noted in many locations along the Estonian coast (Tõnisson et al. 2020), as well as in other areas in Europe (Clemmensen et al. 2015; Jackson et al. 2019). A sharp charcoal-rich humic layer, dating to ~1270 CE, separates sandy layers dating to 590 and 1630 CE (Fig. 8). It indicates that, at least at the AO site, a forest fire may have destroyed vegetation and facilitated the development of the aeolian layer sometime between 1270 and 1630 CE. Quite possibly, the

blowout visible in the background of Fig. 8 occurred later. However, the extent and wider impact of the event marked by the charcoal date at ~1270 CE remain unknown. Forest fires of this kind likely occurred repeatedly during the Late Holocene (e.g. Kuosmanen et al. 2018). An earlier aeolian sand influx (ASI)-based storminess reconstruction from a bog near Lake Järve (Fig. 2) showed higher ASI values around 200 BCE–50 CE, 900–1000 CE, 1100–1300 CE, and during the last 500 years (Vandel et al. 2019; Vaasma et al. 2025). Although it is difficult to directly compare studies conducted using different methods and resolutions, the periods of increased storminess around 1000–1300 CE and during the LIA appear to align.

It has been widely discussed that the LIA resulted in large-scale transgressive coastal dune behaviour and manifested in a relocation of sand in coastal zone throughout Europe (Jackson et al. 2019). Several mechanisms may have been intertwined, including those of climatic and anthropogenic background. Specifically, in the Baltic Sea area, the large dune ridge on the Curonian Spit (Lithuania) formed only from the 16th century onwards, largely due to destructive human practices and forest fires (Dobrotin et al. 2013). Quite similarly, the removal of some vegetation from the frontal dunes at Skagen Peninsula (Denmark) by local inhabitants during the early and middle part of the LIA made the dunes vulnerable to remobilisation. It is also known that King Christian III of Denmark promulgated a law in 1539 CE forbidding the removal of vegetation from the dunes, implying that dune vegetation may have been partly destroyed during the LIA (Clemmensen et al. 2015).

In Estonia, it has been suggested that anthropogenic deforestation in the Järve area, driven by population growth, the construction of the nearby Kuressaare Episcopal Castle (~1380 CE), and increased marine transport, may have contributed to dune formation (Luik et al. 2025). The need for additional firewood to cope with the cooling climate could have further accelerated forest cutting. In addition, slash-and-burn agriculture, which frequently resulted in widespread forest fires, was a common technique in medieval Europe, including Estonia (Jääts et al. 2010). Rapid deforestation is evidenced, for instance, by a 1297 law prohibiting coastal forest cutting near Tallinn (Etverk 1997). Fire cultivation and extensive forest cutting only declined considerably in Estonia by the 19th century (Jääts et al. 2010).

As previously discussed, although the ridges along the Järve coast are sandy, wind-blown dunes are practically missing at the Järve outcrop (MO) location. Aeolian contributions to the landscape are sporadic. Despite traditional names found in the area – Järve dunes (*Järve luited* in Estonian) or Mändjala dunes (*Mändjala luited*) – the landform is predominantly not of aeolian origin. The Järve spit (or coastal barrier) system is mainly marine-built. The difference between the gently bending palaeospits shaped by marine processes and the 'rougher' aeolian landforms is noticeable on the digital elevation model (Fig. 2). The aeolian layer is relatively thin, and the impression of dunes occurs only in a few reblown locations near the current coastline, where (marine) sand has been reworked and blown upwards (on top

of a 4–5-m high marine ridge), reaching 10.8 m above mean sea level. Another blowout at Mändjala (7.6 m elevation; Fig. 1) contributed 2–3 m in thickness.

Finally, the past ~100–150 years (Fig. 9D) have been characterised by a growing sediment deficit at the Järve site (Luik et al. 2025). The Järve barrier, now mostly 4–5 m high, is eroding along its seaward side (Orviku 2006; Tõnisson et al. 2024a). The eroded material has been transported northeast towards Mändjala and Nasva (Fig. 2). A similar longshore sediment transport pattern, generally directed from southwest to northeast by prevailing winds, waves, and coastline configuration, can also be observed on the Latvian side of the Gulf of Riga (Soomere et al. 2025). It is difficult to assess the total recession (i.e. the extent of land loss), but in total it may reach ~100–200 m at Järve. Aerial photos document up to 75 m of shoreline recession between 1956 and 2023, and 20 m of scarp recession (Luik et al. 2025). The erosion-prone, scarped coastal section is currently 2–3 km long at Järve, but it is expected to lengthen as relative sea level rises and the duration of protective seasonal sea-ice cover continues to diminish.

5. Conclusions

1. The seaward section of the Järve palaeospit, where the studied scarp is located, began to emerge approximately 1600 years ago in front of the older spit system dating back 3500–4000 years. It has grown in height and volume due to both sediment accretion and postglacial uplift, which alone has raised it by ~3.5 m over the past 1600 years.

2. A comparison of OSL and radiocarbon (^{14}C) dates from the scarp revealed that seashells are not reliable for dating in coastal stratigraphic studies, particularly on shores with prevailing longshore sediment transport. Shells may be displaced by storm waves and reworked through cycles of deposition and erosion. In addition, the obtained ages can be influenced by the marine reservoir effect and the hard-water effect. These influences may act simultaneously at the Järve site and point to a more general issue. Further site-specific studies are needed to better quantify these effects or to avoid seashell-based dating altogether.

3. Stratigraphic and granulometric analyses showed that the lower part of the examined outcrop (now at 0.8–1.4 m elevation) was formed by sediment accumulation in a shallow (1–3-m deep) nearshore seabed, possibly atop an underwater bar. Cross-bedded laminae indicated fluctuating energy conditions and a rapid expansion of the spit in both width and length, extending towards Mändjala. The elongation of the raised sandy spit is also visible in the GPR imagery. Darker or coarser material streaks and variations in lamination patterns point to changes in sediment provenance and environmental forcing, including storm activity. Above the marine-deposited spit layers, a thin aeolian layer is present, though it is intermixed with paedogenic processes at the Järve site. Owing to the raised-beach setting, it was possible to detect changes in forcing conditions even within the underwater formations at Järve.

4. The activation of aeolian processes and sand redistribution during the Little Ice Age (~1300–1850 CE), a phenomenon observed along many European coasts, had only a limited impact at Järve. Despite traditional place names such as Järve dunes and Mändjala dunes, the coastal landforms are predominantly of marine origin. The Järve coastal barrier system was primarily built by marine processes, whereas the upper aeolian layer is thin and patchy, with dune-like features appearing only in a few isolated blowout areas. In one such location, marine sand was reblown into a dune reaching a height of 5 m (10.8 m above sea level). These blowouts were attributed to the colder climate of the Little Ice Age and anthropogenic disturbances to vegetation, such as logging or slash-and-burn agriculture.

5. Over the past 100–150 years, the Järve coast has experienced an increasing sediment deficit. The emergent barrier system – composed of older beach ridges and spits, some up to 10 m high – has become erosional. Apparent sea-level lowering has ceased, and both the duration and extent of seasonal sea ice have declined. While it is difficult to quantify the total extent of coastal recession (i.e. the amount of 'lost' land), it may have reached several hundred metres at Järve. The eroded sediments have been transported northeast towards Mändjala and Nasva, where the coastline continues to advance due to ongoing accretion.

6. In addition to the methodological insights regarding seashell-based dating, the broader significance of the study is that it demonstrates how global environmental changes are manifested at a local scale on seacoasts.

Supplementary online data

Supplementary online data to this article can be found at https://doi.org/10.3176/earth.2026.S03 and include Tables S1–S3.

References

Alves, E. Q., Macario, K., Ascough, P. and Bronk Ramsey, C. 2018. The worldwide marine radiocarbon reservoir effect: definitions, mechanisms, and prospects. *Reviews of Geophysics*, **56**(1), 278–305. https://doi.org/10.1002/2017RG000588

Andrén, T., Björck, S., Andrén, E., Conley, D., Zillén, L. and Anjar, J. 2011. The development of the Baltic Sea basin during the last 130 ka. In *The Baltic Sea Basin* (Harff, J., Björck, S. and Hoth, P., eds). Springer, Berlin, Heidelberg, 75–97. https://doi.org/10.1007/978-3-642-17220-5_4

Ascough, P. L., Cook, G. T. and Dugmore, A. 2005. Methodological approaches to determining the marine radiocarbon reservoir effect. *Progress in Physical Geography*, **29**(4), 532–547. http://eprints.gla.ac.uk/5017

Blott, S. J. and Pye, K. 2001. Gradistat: a grain size distribution and statistics package for the analysis of unconsolidated sediments. *Earth Surface Processes and Landforms*, **26**(11), 1237–1248. https://doi.org/10.1002/esp.261

Buylaert, J. P., Murray, A. S., Thomsen, K. J. and Jain, M. 2009. Testing the potential of an elevated temperature IRSL signal from K-feldspar. *Radiation Measurements*, **44**(5–6), 560–565. https://doi.org/10.1016/j.radmeas.2009.02.007

Buynevich, I. V., FitzGerald, D. M. and van Heteren, S. 2004. Sedimentary records of intense storms in Holocene barrier sequences, Maine, USA. *Maine Geology*, **210**(1–4), 135–148. https://doi.org/10.1016/j.margeo.2004.05.007

Buynevich, I. V., Tõnisson, H., Suursaar, Ü., Pupienis, D., Davydov, O. V., Kont, A. et al. 2023. Diverse erosional indicators along a rapidly retreating Holocene strandplain margin, leeward Hiiumaa Island, Estonia. *Baltica*, **36**(1), 79–88. https://doi.org/10.5200/baltica.2023.1.7

Buynevich, I. V., Tõnisson, H., Pupienis, D., Rosentau, A., Bitinas, A., Jarmalavičius, D. et al. 2024. High-resolution sampling and rapid image-based assessment of dark opaque fractions in coastal sands. *Journal of Coastal Research*, **113**(SP1), 778–782. https://doi.org/10.2112/JCR-SI113-153.1

Clemmensen, L. B., Glad, A. C., Hansen, K. W. T. and Murray, A. S. 2015. Episodes of aeolian sand movement on a large spit system (Skagen Odde, Denmark) and North Atlantic storminess during the Little Ice Age. *Bulletin of the Geological Society of Denmark*, **63**, 17–28. https://doi.org/10.37570/bgsd-2015-63-03

Costas, S. 2022. Evolutionary trajectories of coastal sand barriers along the West Portuguese coast during the Holocene. *Journal of Marine Science and Engineering*, **10**(12), 1894. https://doi.org/10.3390/jmse10121894

Dearing, J. A. 1999. *Environmental Magnetic Susceptibility: Using the Bartington MS2 System*. 2nd ed. Chi Publishers, Kenilworth.

Dobrotin, N., Bitinas, A., Michelevičius, D., Damušyte, A. and Mažeika, J. 2013. Reconstruction of the Dead (Grey) Dune evolution along the Curonian Spit, southeastern Baltic. *Bulletin of the Geological Society of Finland*, **85**, 53–64. https://doi.org/10.17741/bgsf/85.1.004

Dougherty, A. J. 2014. Extracting a record of Holocene storm erosion and deposition preserved in the morphostratigraphy of a prograded coastal barrier. *Continental Shelf Research*, **86**, 116–131. https://doi.org/10.1016/j.csr.2013.10.014

Durcan, J. A., King, G. E. and Duller, G. A. T. 2015. DRAC: Dose Rate and Age Calculator for trapped charge dating. *Quaternary Geochronololgy*, **28**, 54–61. https://doi.org/10.1016/j.quageo.2015.03.012

Eberhards, G. and Saltupe, B. 1995. Accelerated coastal erosion – implications for Latvia. *Baltica*, **9**, 16–28.

ELB (Estonian Land Board). 2025a. *Geological data*. https://xgis.maaamet.ee/xgis2/page/app/geoloogia400k (accessed 2025-04-01).

ELB (Estonian Land Board). 2025b. *Elevation data*. http://geo portaal.maaamet.ee/eng/Maps-and-Data/Topographicdata/Elevation-data-p308.html (accessed 2025-04-01).

ELB (Estonian Land Board). 2025c. *Historic maps*. https://xgis.maaamet.ee/xgis2/page/app/ajalooline (accessed 2025-04-01).

ELB (Estonian Land Board). 2025d. *Photo storage*. https://fotoladu.maaamet.ee (accessed 2025-04-01).

Etverk, I. 1997. Lisamõtteid Anno Domini 1297 juurde (Additional thoughts on 'Anno Domini 1297'). *Eesti Mets*, **2**, 10–11.

EWS (Estonian Weather Service). 2025. *Coastline stations*. https://www.ilmateenistus.ee/meri/vaatlusandmed/kogu-rannik/kaart/?lang=en (accessed 2025-04-01).

Furmanczyk, K. and Musielak, S. 2002. Important features of coastline dynamics in Poland: "nodal points" and "gates". In *Baltic Coastal Ecosystems. Central and Eastern European Development Studies* (Schernewski, G. and Schiewer, U., eds). Springer, Berlin, Heidelberg, 141–147. https://doi.org/10.1007/978-3-662-04769-9_10

Galbraith, R. F., Roberts, R. G., Laslett, G. M., Yoshida, H. and Olley, J. M. 1999. Optical dating of single and multiple grains of quartz from Jinmium rock shelter, northern Australia: part I, experimental design and statistical models. *Archaeometry*, **41**(2), 339–364. https://doi.org/10.1111/j.1475-4754.1999.tb00987.x

Hang, T., Veski, S., Vassiljev, J., Poska, A., Kriiska, A. and Heinsalu, A. 2020. A new formal subdivision of the Holocene Series/Epoch in Estonia. *Estonian Journal of Earth Sciences*, **69**(4), 269–280. https://doi.org/10.3176/earth.2020.15

Harff, J., Jöns, H. and Rosentau, A. 2020. Geological, paleoclimatological, and archaeological history of the Baltic Sea region since the last glaciation. In *Oxford Research Encyclopedia of Climate Science*. Oxford University Press, Oxford, 1–50. https://doi.org/10.1093/acrefore/9780190228620.013.621

Hedenström, A. and Possnert, G. 2001. Reservoir ages in Baltic Sea sediment – a case study of an isolation sequence from the Litorina Sea stage. *Quaternary Science Reviews*, **20**(18), 1779–1785. https://doi.org/10.1016/S0277-3791(01)00069-5

IPCC. 2021. *AR6 Climate Change 2021: The Physical Science Basis*. https://www.ipcc.ch/report/ar6/wg1 (accessed 2025-04-01).

Jaagus, J. and Suursaar, Ü. 2013. Long-term storminess and sea level variations on the Estonian coast of the Baltic Sea in relation to large-scale atmospheric circulation. *Estonian Journal of Earth Sciences*, **62**(2), 73–92. https://doi.org/10.3176/earth.2013.07

Jääts, L., Kihno, K., Tomson, P. and Konsa, M. 2010. Tracing fire cultivation in Estonia. *Forestry Studies*, **53**, 53–65. https://doi.org/10.2478/v10132-011-0089-3

Jackson, D. W. T., Costas, S. and Guisado-Pintado, E. 2019. Large-scale transgressive coastal dune behaviour in Europe during the Little Ice Age. *Global and Planetary Change*, **175**, 82–91. https://doi.org/10.1016/j.gloplacha.2019.02.003

Kalińska, E., Weckwerth, P., Lamsters, K., Alexanderson, H., Martewicz, J. and Rosentau, A. 2024. Paleostorm redeposition and post-glacial coastal chronology in the eastern Baltic Sea, Latvia. *Geomorphology*, **467**, 109456. https://doi.org/10.1016/j.geomorph.2024.109456

Kalm, V. 2006. Pleistocene chronostratigraphy in Estonia, southeastern sector of the Scandinavian glaciation. *Quaternary Science Reviews*, **25**(9–10), 960–975. https://doi.org/10.1016/j.quascirev.2005.08.005

Kreutzer, S., Burow, C., Dietze, M., Fuchs, M. C., Schmidt, C., Fischer, M. et al. 2025. Luminescence: Comprehensive Luminescence Dating Data Analysis. R package version 1.1.0. https://CRAN.R-project.org/package=Luminescence (accessed 2025-04-01).

Kuosmanen, N., Marquer, L., Tallavaara, M., Molinari, C., Zhang, Y., Alenius, T. et al. 2018. The role of climate, forest fires and human population size in Holocene vegetation dynamics in Fennoscandia. *Journal of Vegetation Science*, **29**(3), 382–392. https://doi.org/10.1111/jvs.12601

Long, A. J., Strzelecki, M. C., Lloyd, J. M. and Bryant, C. L. 2012. Dating High Arctic Holocene relative sea level changes using juvenile articulated marine shells in raised beaches. *Quaternary Science Reviews*, **48**, 61–66. https://doi.org/10.1016/j.quascirev.2012.06.009

Lougheed, B. C., Filipsson, H. L. and Snowball, I. 2013. Large spatial variations in coastal ^{14}C reservoir age – a case study from the Baltic Sea. *Climate of the Past*, **9**(3), 1015–1028. https://doi.org/10.5194/cp-9-1015-2013

Luik, K., Suursaar, Ü., Tõnisson, H., Rivis, R., Suuroja, S. and Vilumaa, K. 2024a. Millennia-long progradation turned into coastal erosion at Järve coast of the Baltic Sea. *Journal of Coastal Research*, **113**(SP1), 235–239. https://doi.org/10.2112/JCR-SI113-047.1

Luik, K., Tõnisson, H., Rivis, R., Vilumaa, K., Vaasma, T., Vandel, E. et al. 2024b. *Geomorphology of the Järve coast (Saaremaa Island, Estonia)*. Dataset. https://doi.org/10.23673/re-484

Luik, K., Tõnisson, H., Rivis, R., Vilumaa, K., Vaasma, T., Vandel, E. et al. 2025. Development shifts on the emerging Järve coast (Estonia) in Late Holocene. *Marine Geology*, **481**, 107478. https://doi.org/10.1016/j.margeo.2025.107478

Morton, R. A., Miller, T. L. and Moore, L. J. 2004. *National Assessment Of Shoreline Change: Part 1, Historical Shoreline Changes and Associated Coastal Land Loss Along the U.S. Gulf of Mexico*. https://pubs.usgs.gov/publication/ofr20041043

Murray, A. S. and Wintle, A. G. 2000. Luminescence dating of quartz using an improved single-aliquot regenerative-dose protocol. *Radiation Measurements*, **32**(1), 57–73. https://doi.org/10.1016/S1350-4487(99)00253-X

Murray, A. S. and Wintle, A. G. 2003. The single aliquot regenerative dose protocol: potential for improvements in reliability. *Radiation Measurements*, **37**(4–5), 377–381. https://doi.org/10.1016/S1350-4487(03)00053-2

Murray, A., Arnold, L. J., Buylaert, J.-P., Guérin, G., Qin, J., Singhvi, A. K. et al. 2021. Optically stimulated luminescence dating using quartz. *Nature Reviews Methods Primers*, **1**, 72. https://doi.org/10.1038/s43586-021-00068-5

Muru, M., Rosentau, A., Preusser, F., Plado, J., Sibul, I., Jõeleht, A. et al. 2018. Reconstructing Holocene shore displacement and Stone Age palaeogeography from a foredune sequence on Ruhnu Island, Gulf of Riga, Baltic Sea. *Geomorphology*, **303**, 434–445. https://doi.org/10.1016/j.geomorph.2017.12.016

Najafzadeh, F. and Soomere, T. 2024. Impact of changes in sea ice cover on the wave climate of semi-enclosed, seasonally ice-covered water bodies at temperate latitudes: a case study in the Gulf of Riga. *Estonian Journal of Earth Sciences*, **73**(1), 26–36. https://doi.org/10.3176/earth.2024.03

Najafzadeh, F., Jankowski, M. Z., Giudici, A., Männikus, R., Suursaar, Ü., Viška, M. et al. 2024. Spatiotemporal variability of wave climate in the Gulf of Riga. *Oceanologia*, **66**(1), 56–77. https://doi.org/10.1016/j.oceano.2023.11.001

Nirgi, T., Grudzinska, I., Kalińska, E., Konsa, M., Jõeleht, A., Alexanderson, H. et al. 2022. Late-Holocene relative sea-level changes and palaeoenvironment of the Pre-Viking Age ship burials in Salme, Saaremaa Island, eastern Baltic Sea. *The Holocene*, **32**(4), 237–253. https://doi.org/10.1177/09596836211066596

Orviku, K. 2006. Development ties between Järve-Mändjala beach and Nasva harbour. *Proceedings of the Estonian Maritime Academy*, **3**, 7–18.

Pupienis, D., Buynevich, I., Ryabchuk, D., Jarmalavičius, D., Žilinskas, G., Fedorovič, J. et al. 2017. Spatial patterns in heavy-mineral concentrations along the Curonian Spit coast, southeastern Baltic Sea. *Estuarine, Coastal and Shelf Science*, **195**, 41–50. https://doi.org/10.1016/j.ecss.2016.08.008

Ratas, U., Rivis, R., Truus, L., Vilumaa, K., Multer, R. and Anderson, A. 2011. The aeolian coastal ecosystems of Estonia and their changes. *Journal of Coastal Research*, **64**(SI), 430–434.

Raukas, A. 2000. Rapid changes of the Estonian coast during the late glacial and Holocene. *Marine Geology*, **170**(1–2), 169–175. https://doi.org/10.1016/S0025-3227(00)00072-4

Reimer, P. J., Austin, W. E. N., Bard, E., Bayliss, A., Blackwell, P. G., Bronk Ramsey, C. et al. 2020. The IntCal20 Northern Hemisphere radiocarbon age calibration curve (0–55 cal kBP). *Radiocarbon*, **62**(4), 725–757. https://doi.org/10.1017/RDC.2020.41

Roberts, H. M. and Wintle, A. G. 2001. Equivalent dose determinations for polymineralic fine-grains using the SAR protocol: application to a Holocene sequence of the Chinese Loess Plateau. *Quaternary Science Reviews*, **20**(5–9), 859–863. https://doi.org/10.1016/S0277-3791(00)00051-2

Rosentau, A., Vassiljev, J., Hang, T., Saarse, L. and Kalm, V. 2009. Development of the Baltic Ice Lake in the eastern Baltic. *Quaternary International*, **206**(1–2), 16–23. https://doi.org/10.1016/j.quaint.2008.10.005

Rosentau, A., Jõeleht, A., Plado, J., Aunap, R., Muru, M. and Eskola, K. O. 2013. Development of the Holocene foredune plain in the Narva-Jõesuu area, eastern Gulf of Finland. *Geological Quarterly*, **57**(1), 89–100.

Rosentau, A., Nirgi, T., Muru, M., Bjursäter, S., Hang, T., Preusser, F. et al. 2020. Holocene relative shore level changes and Stone Age hunter-gatherers in Hiiumaa Island, eastern Baltic Sea. *Boreas*, **49**(4), 783–798. https://doi.org/10.1111/bor.12452

Różyński, G. 2023. Coastal protection challenges after heavy storms on the Polish coast. *Continental Shelf Research*, **266**, 105080. https://doi.org/10.1016/j.csr.2023.105080

Saarse, L., Vassiljev, J. and Rosentau, A. 2009. Ancylus Lake and Litorina Sea transition on the Island of Saaremaa, Estonia: a pilot study. *Baltica*, **22**(1), 51–62.

Soomere, T., Jankowski, M. Z., Eelsalu, M., Parnell, K. E. and Viška, M. 2025. Alongshore sediment transport analysis for a semi-enclosed basin: a case study of the Gulf of Riga, the Baltic Sea. *Ocean Science*, **21**(2), 619–641. https://doi.org/10.5194/os-21-619-2025

Suuroja, S., Veski, A., Liira, M., Tuuling, I. and Ausmeel, M. 2020. *2019.–2020. aasta mererannikute seire tööd (Coastal monitoring work in 2019–2020)*. Aruanne. Eesti Geoloogiateenistus, Rakvere. https://kese.envir.ee/kese/downloadReportFile.action?fileUid=20443975&monitoringWorkUid=17723750 (accessed 2025-04-01).

Suursaar, Ü. 2023. Variations in wind velocity components and average air flow properties at Estonian coastal stations in 1966–2021; Sõrve Peninsula case study. *Estonian Journal of Earth Sciences*, **72**(2), 197–210. https://doi.org/10.3176/earth.2023.85

Suursaar, Ü. and Kall, T. 2018. Decomposition of relative sea level variations at tide gauges using results from four Estonian precise levelings and uplift models. *IEEE Journal of Selected Topics in Applied Earth Observations and Remote Sensing*, **11**(6), 1966–1974. https://doi.org/10.1109/JSTARS.2018.2805833

Suursaar, Ü., Kullas, T., Otsmann, M., Saaremäe, I., Kuik, J. and Merilain, M. 2006. Cyclone Gudrun in January 2005 and modelling its hydrodynamic consequences in the Estonian coastal waters. *Boreal Environment Research*, **11**, 143–159. https://www.borenv.net/BER/archive/pdfs/ber11/ber11-143.pdf

Suursaar, Ü., Jaagus, J. and Tõnisson, H. 2015. How to quantify long-term changes in coastal sea storminess? *Estuarine, Coastal and Shelf Science*, **156**, 31–41. https://doi.org/10.1016/j.ecss.2014.08.001

Suursaar, Ü., Rosentau, A., Hang, T., Tõnisson, H., Tamura, T., Vaasma, T. et al. 2022. Climatically induced cyclicity recorded in the morphology of uplifting Tihu coastal ridgeplain, Hiiumaa Island, eastern Baltic Sea. *Geomorphology*, **404**, 108187. https://doi.org/10.1016/j.geomorph.2022.108187

Suursaar, Ü., Torn, K., Mäemets, H. and Rosentau, A. 2024. Overview and evolutionary path of Estonian coastal lagoons. *Estuarine Coastal and Shelf Science*, **303**, 108811. https://doi.org/10.1016/j.ecss.2024.108811

Suursaar, Ü., Luik, K., Mäll, M., Jaagus, J. and Tõnisson, H. 2025. Long-term variations in sea ice extent can influence trends in maximum sea level in the northeastern Baltic Sea. *Continental Shelf Research*, **289**, 105451. https://doi.org/10.1016/j.csr.2025.105451

Tamura, T. 2012. Beach ridges and prograded beach deposits as palaeoenvironment records. *Earth-Science Reviews*, **114**(3–4), 279–297. https://doi.org/10.1016/j.earscirev.2012.06.004

Tarand, A., Jaagus, J. and Kallis, A. 2013. *Eesti kliima minevikus ja tänapäeval (Estonian Climate, Past and Present)*. University of Tartu Press, Tartu.

Tõnisson, H., Orviku, K., Jaagus, J., Suursaar, Ü., Kont, A. and Rivis, R. 2008. Coastal damages on Saaremaa Island, Estonia, caused by the extreme storm and flooding on January 9, 2005. *Journal of Coastal Research*, **24**(3), 602–614. https://doi.org/10.2112/06-0631.1

Tõnisson, H., Suursaar, Ü., Rivis, R., Tamura, T., Aarna, T., Vilumaa, K. et al. 2020. Characteristics and formation of a solitary dune belt encountered along the coast of Estonia. *Journal of Coastal Research*, **95**(SP1), 689–694. https://doi.org/10.2112/SI95-134.1

Tõnisson, H., Männikus, R., Vaasma, T. and Rohumägi, K. 2022. *Nasva sadama tuuliku mõju setete liikumisele ja heljumi levik süvendamisel (The effect of the Nasva harbour windmill on sediment transport and turbidity dispersion during dredging)*. Report. Tallinn University, Institute of Ecology, Tallinn.

Tõnisson, H., Kont, A., Suursaar, Ü., Jaagus, J., Rivis, R. and Buynevich, I. 2024a. Morphosedimentary evolution of Estonian coastline: role of climatic and hydrodynamic forcing over the past decades. *Boreal Environment Research*, **29**(1–6), 103–125. https://www.borenv.net/BER/archive/pdfs/ber29/ber29-103-125.pdf

Tõnisson, H., Luik, K., Suursaar, Ü., Buynevich, I., Kont, A., Männikus, R. et al. 2024b. Rapidly transforming Holocene strandplain, affected by port jetty and hydroclimatic shifts – natural laboratory of past and future shoreline behavior. *Journal of Coastal Research*, **113**(SP1), 715–719. https://doi.org/10.2112/JCR-SI113-141.1

Tõnisson, H., Männikus, R., Kont, A., Palginõmm, V., Alari, V., Suuroja, S. et al. 2024c. Application of shore sediments accumulated in navigation channel for restoration of sandy beaches around Pärnu city, SW Estonia, Baltic Sea. *Journal of Marine Science and Engineering*, **12**(3), 394. https://doi.org/10.3390/jmse12030394

Tudyka, K., Miłosz, S., Adamiec, G., Bluszcz, A., Poręba, G., Paszkowski, Ł. et al. 2018. μDose: a compact system for environmental radioactivity and dose rate measurement. *Radiation Measurements*, **118**, 8–13.

Uścinowicz, G., Uścinowicz, S., Szarafin, T., Maszloch, E. and Wirkus, K. 2024. Rapid coastal erosion, its dynamics and cause – an erosional hot spot on the southern Baltic Sea coast. *Oceanologia*, **66**(2), 250–266. https://doi.org/10.1016/j.oceano.2023.12.002

Vaasma, T., Vandel, E., Sugita, S., Tõnisson, H., Suursaar, Ü., Kont, A. et al. 2025. Storminess reconstruction in the northeastern Baltic Sea region over the past 7600 years based on aeolian sand influx into coastal bogs. *The Holocene*, **35**(1), 61–74. https://doi.org/10.1177/09596836241285783

Vandel, E., Vaasma, T., Sugita, S., Tõnisson, H., Jaagus, J., Vilumaa, K. et al. 2019. Reconstruction of past storminess: evaluation of an indicator approach using aeolian mineral grains buried in peat deposits, Estonia. *Quaternary Science Reviews*, **218**, 215–227. https://doi.org/10.1016/j.quascirev.2019.06.026

Vestøl, O., Ågren, J., Steffen, H., Kierulf, H. and Tarasov, L. 2019. NKG2016LU: a new land uplift model for Fennoscandia and the Baltic Region. *Journal of Geodesy*, **93**, 1759–1779. https://doi.org/10.1007/s00190-019-01280-8

Vilumaa, K., Ratas, U., Tõnisson, H., Kont, A. and Pajula, R. 2017. Multidisciplinary approach to studying the formation and development of beach-ridge systems on non-tidal uplifting

coasts in Estonia. *Boreal Environment Research*, **22**, 67–81. https://www.borenv.net/BER/archive/pdfs/ber22/ber22-067-081-Vilumaa.pdf

Weisse, R., Dailidienė, I., Hünicke, B., Kahma, K., Madsen, K., Omstedt, A. et al. 2021. Sea level dynamics and coastal erosion in the Baltic Sea region. *Earth System Dynamics*, **12**(3), 871–898. https://doi.org/10.5194/esd-12-871-2021

Willis, J., Hamlington, B. and Fournier, S. 2024. *Global Mean Sea Level, Trajectory and Extrapolation*. https://doi.org/10.5281/zenodo.7702314 (accessed 2025-04-01).

Akumulatsiooni- ja erosioonisündmuste morfostratigraafia ning kronoloogia Järve rannajärsakul (Saaremaal, Lääne-Eestis) viimase 2000 aasta jooksul

Ülo Suursaar, Katre Luik, Alar Rosentau, Helena Alexanderson, Reimo Rivis, Tiit Vaasma, Egert Vandel, Kadri Vilumaa, Donatas Pupienis ja Hannes Tõnisson

Kliimamuutuse ja meretaseme tõusu koosmõjul toimuvad paljudes maailma paikades mererannikutel režiiminihked, näiteks Läänemere lõuna- ja kaguosas on suurenenud rannikuerosioon. Uuring rekonstrueerib Järve rannajärsaku setete ladestumise ja erosiooni ajaloo, kasutades uusi luminestsents- ja radiosüsiniku vanusemääranguid, georadari ja LiDARi kõrgusandmeid ning paljandi litoloogilist kirjeldust. Merepoolne rannavall, kus praegu asub uuritud 3,5 meetri kõrgune liivadesse tekkinud järsak, hakkas kujunema jääajajärgse maakerke ja setete kuhjumise tulemusena 3500–4000 aasta vanuse maasääre ette umbes 1600 aastat tagasi. Paljandi alumine osa settis madalas rannavööndis rannabarridele. Tumedamad settekihid ja litoloogilise koostise varieerumine peegeldavad muutusi settimistingimustes ja tormide aktiivsuses. Mereliste protsesside tagajärjel kuhjunud liivakihtide ülaosas asub õhuke eoolne kiht, mis on konkreetses paljandis nõrgalt arenenud. Luitelised pinnavormid esinevad Järve–Mändajala piirkonnas vaid mõnes üksikus nn ümberpuhutud kohas, mis on tõenäoliselt seotud väikese jääaja (~1300–1850 AD) külmema kliima ja inimtekkelise taimestiku kahjustamisega, nagu metsaraie või alepõllundus. Viimase ~100 aasta jooksul on varem kerkinud ja laienenud rannavallide ja maasäärte süsteem muutunud erosiooniliseks. Varasem suhtelise meretaseme langus on peatunud, talvist merejääd on üha vähem ning seetõttu on talvetormide mõju tugevam ja järsak taandub. Uuring demonstreerib, kuidas globaalsed muutused avalduvad mererannikul kohalikul tasandil, tuues ühtlasi esile merekarpide kasutamisega seotud metodoloogilised raskused rannikualade stratigraafilisel dateerimisel.